

https://dspace.org/

# The potential of medical imaging modalities to identify a concealed energetic materials device

**Mngqete, Samkelo**

**2018**

https://hdl.handle.net/10539/25631

Mngqete, Samkelo (2018) The potential of medical imaging modalities to identify a concealed energetic materials device, University of the Witwatersrand, Johannesburg, https://hdl.handle.net/10539/25631

Downloaded from a DSpace repository. https://dspace.org/

UNIVERSITY OF THE WITWATERSRAND
JOHANNESBURG

FACULTY OF SCIENCE




# THE POTENTIAL OF MEDICAL IMAGING MODALITIES TO IDENTIFY A CONCEALED ENERGETIC MATERIALS DEVICE

Samkelo Mngqete

A Research Report submitted to the Faculty of Science, University of the Witwatersrand, Johannesburg, in partial fulfilment of the requirements for the degree of Master of Science

Johannesburg
2018

# DECLARATION

I declare that this Research Report is my own, unaided work. It is being submitted for the Degree of Master of Science at the University of the Witwatersrand, Johannesburg. It has not been submitted before for any degree or examination at any other University.

I certify that this research work has a waiver of ethics clearance from the Human Research Ethics Committee (Medical) at the University of the Witwatersrand. (Ref: W-CJ-160505-2)



_____
(Signature of candidate)

5th day of February 20 18 in Braamfontein

# ABSTRACT

The act of terrorism has received much attention in recent years. In this study, a technique was investigated to identify concealed energetic materials which could aid in reducing the threat of terrorism and save innocent lives. Using different X-ray source and detector technologies for imaging, a variety of medical imaging modalities in Charlotte Maxeke Academic Hospital (CMJAH) are investigated as a potential to identifying concealed materials.

An inert dummy improvised explosive device (IED) was built in the form of a handheld briefcase. The IED and an Electronic Portal Imaging Device (EPID) Quality Control (QC) phantom were imaged using the Toshiba medical simulator, Orthovoltage teletherapy machine, Cobalt 60 ($^{60}$Co) teletherapy machine, Linear Accelerator (Linac), and Computed Tomography (CT) scanner. Detection methods used were Kodak X-Omat V ready pack film, Fuji medical X-ray film, Gafchromic film, and an EPID.

The low energy from the simulator was absorbed by the high-density materials in the briefcase. The image had high contrast, and since this was planar imaging hidden, materials were not visible. The CT scanner contained many streak artefacts, producing poor 3D images of the briefcase. At high energies the Linac and $^{60}$Co teletherapy machine penetrated through the thick materials, displaying underlying and overlying materials on the image. The modality which had the best balance between contrast and spatial resolution was the orthovoltage teletherapy machine.

The orthovoltage teletherapy machine, being the only modality to display all the materials of the IED has the potential to be used as a modality to identify a concealed energetic materials device.

# DEDICATION

*In Loving Memory of my Grandfather*

*Vuyisile Johnson Mngqete*

*1927 – 2016*

*To my Daughter Zukhanye Sisipho Konke Bidla*

*To my Mother, Nolizo Mngqete*

*To my Family (Mkhwananzi, Khweba, Nzala, Zotsho), thank you for the constant love and support throughout my studies.*

*Moreover, to the Mzizi Family, I appreciate everything you have done for me.*

# ACKNOWLEDGEMENTS

First and foremost, I would like to give thanks and praise to the Most High God, for the good health and strength provided to compile this report.

My supervisors Prof D Van Der Merwe and Dr T Sono, thank you for the invaluable and profound guidance and expertise provided to me. To the Charlotte Maxeke Johannesburg Academic Hospital (CMJAH) Medical Physics Department, I would like to humbly thank you for lending me your resources, with immense gratitude.

To the Armaments Corporation of South Africa (ARMSCOR) and the Council of Scientific and Industrial Research (CSIR) thank you for sponsoring my studies, this allowed me to live very close to my dreams.

I would like to thank Mr L. C Nethwadzi for the discussions and advice given over the course of this report.

I am particularly grateful to Mr K. Mahlangu and Mr L. Nobecu for the assistance given when taking measurements.

I would like to express my very great appreciation to Ms T K Bidla for the continuous support and encouragement throughout my studies.

# TABLE OF CONTENTS

Declaration ..... ii

Abstract ..... iii

Dedication ..... iv

Acknowledgements ..... v

List of Figures ..... viii

List of Tables ..... x

Nomenclature ..... xi

1. Introduction ..... 1

1.1 Background ..... 1

1.2 Problem Statement ..... 3

1.3 Research aim ..... 4

1.4 General objectives ..... 4

2. Literature review and theoretical framework ..... 5

2.1 Explosives detection systems ..... 7

2.1.1 X-ray interaction with matter ..... 7

2.1.2 Photon screening methods ..... 9

2.1.3 Nuclear technology based explosives detection ..... 11

2.1.4 Laser based explosives detection ..... 12

2.2 Theoretical framework of imaging ..... 12

2.2.1 Film ..... 12

2.2.2 Digital detectors ..... 14

2.2.3 Image quality ..... 15

3. Methodology ..... 17

3.1 Modalities ..... 21

3.2 Summary of experimental procedure ..... 28

4. Results and Discussion ..... 29
4.1 EPID QC phantom imaging ..... 29
4.2 Briefcase imaging ..... 33
4.2.1 Radiotherapy simulator imaging ..... 33
4.2.2 Linear accelerator ..... 36
4.2.3 Cobalt-60 ..... 39
4.2.4 Orthovoltage ..... 42
4.2.5 CT ..... 47
4.3 Summary table of results ..... 48
5. Conclusion ..... 49
6. Recommendations ..... 50
7. References ..... 51

# LIST OF FIGURES

Figure 1: A flow diagram showing the stages of the development and implications of an IED. ..... 3

Figure 2: A schematic diagram showing essential IED components. ..... 5

Figure 3: A schematic diagram of a commercial electric detonator. ..... 6

Figure 4: An illustration of the Compton effect (from [27]). ..... 8

Figure 5: A diagram showing the cross-section of radiographic film. ..... 13

Figure 6: An image of the dummy IED built at the CSIR. ..... 17

Figure 7: a) An image of the PTW EPID QC phantom (from [45]); b) the materials inside the EPID QC phantom (from [48]). ..... 19

Figure 8: An image of the Toshiba medical simulator. ..... 21

Figure 9: A schematic diagram of the Toshiba medical simulator setup used for imaging the briefcase and phantom. ..... 22

Figure 10: A block diagram of a typical medical linear accelerator with an EPID, showing the setup used for imaging the briefcase and phantom. ..... 23

Figure 11: An image of the $^{60}$Co teletherapy machine. ..... 24

Figure 12: A schematic diagram of the imaging setup on the $^{60}$Co teletherapy machine. ..... 24

Figure 13: A schematic diagram of a CT scanner showing the X-ray tube and detector arrays rotate around the object being imaged. ..... 26

Figure 14: A schematic diagram of the setup used to image the phantom and the briefcase on the orthovoltage teletherapy machine. ..... 27

Figure 15: Images of the EPID phantom at the Toshiba medical simulator using Fuji film. The energy and tube current were: a) 40 $kV_p$, 10 mAs; b) 60 $kV_p$, 27.5 mAs, and c) 95 $kV_p$, 10mAs. ..... 29

Figure 16: Images of the EPID phantom radiated at the orthovoltage teletherapy machine using a) 95 $kV_p$, b) 180 $kV_p$ and c) 300 $kV_p$ with Kodak oncology film as a detector. ..... 30

Figure 17: Images of the EPID phantom radiated using the $^{60}Co$ teletherapy machine with a) an exposure time of 0.02 min using Fuji film and b) an exposure time of 0.29 min using the Kodak oncology film. ..... 31

Figure 18: An image of the EPID QC phantom using 6 MV, delivering 2 MU at the Linac using the EPID as a detector. ..... 32

Figure 19: An image from the Toshiba medical simulator with energy and tube current at 40 $kV_p$ and 10 mAs respectively, using Fuji film as a detector. ..... 34

Figure 20: A graph showing optical transmission collected from the Fuji film using the Toshiba medical simulator..... 36

Figure 21: An image of the briefcase using the Linac EPID ..... 37

Figure 22: A graph showing optical transmission from the EPID imager. ..... 39

Figure 23: An image of the briefcase using the $^{60}Co$ teletherapy machine and Fuji film..... 40

Figure 24: A graph showing optical transmission from Fuji film using the $^{60}Co$ teletherapy. ..... 42

Figure 25: An image showing combined Kodak film images from the orthovoltage teletherapy machine at 300 $kV_p$..... 43

Figure 26: An image of the Kodak film displaying the detonator, highlighted in red is the region where the detonator is positioned, traced in green and yellow are the wires connected to the electric match inside the detonator. ..... 45

Figure 27: A graph showing optical transmission on Kodak film using 300 $kV_p$ and 8 mAs, the square box on the graph represents the region where the electric match inside the detonator was located. ..... 46

Figure 28: A cross section of the briefcase using the CT scanner, circled in red is a cross section of the detonator. ..... 47

# LIST OF TABLES

Table 1: A table showing the effective atomic number of materials used in the briefcase..... 18

Table 2: The exposure time and scanning position of each film used in the study.. 25

Table 3: Summary of the experimental procedures used in this study. ..... 28

Table 4: Materials observed using the Toshiba medical simulator. ..... 34

Table 5: Visible materials using the Linac. ..... 37

Table 6: Materials visible using the $^{60}$Co teletherapy machine ..... 41

Table 7: Materials observed using the orthovoltage teletherapy machine. ..... 43

Table 8: A summary table of the visibility of each of the components in the briefcase at each modality. ..... 48

# NOMENCLATURE

| | |
|---|---|
| AOAV | Action on Armed Violence |
| CMJAH | Charlotte Maxeke Johannesburg Academic Hospital |
| $^{60}Co$ | Cobalt-60 |
| CSIR | Council for Scientific and Industrial Research |
| CT | Computed Tomography |
| DICOM | Digital Imaging and Communications in Medicine |
| EPID | Electronic Portal Imaging Device |
| Gy | Gray (1 Gy = 1 J/kg) |
| IED | Improvised Explosive Device |
| $kV_p$ | Peak kilovoltage |
| Linac | Linear accelerator |
| mA | milliampere |
| mAs | milliampere-second |
| MU | Monitor Unit |
| MV | Mega Voltage |
| PETN | Pentaerythritol tetranitrate |
| QA | Quality Assurance |
| QC | Quality Control |
| RDX | Cyclotrimethylenetrinitramine |
| SID | Source to Image Distance |
| SSD | Source to Surface Distance |
| $Z_{eff}$ | Effective atomic number |

# 1. INTRODUCTION

## 1.1 Background

The use of improvised explosive devices (IEDs) dates back to the First World War [1]. An IED is defined as a combination of materials which are not designed or produced to work together, and when assembled, they form a system that has a capability to explode [2]. Improvised weapons are often used by terrorist groups, insurgents, criminals and groups not recognised as a state [3]. Following the PanAm-103 plane bombing in Lockerbie, Scotland in 1988, which was induced by an IED hidden in luggage, there has been a significant focus by scientists into the detection and identification of hidden energetic materials devices [4]. An energetic material is classified as a substance that chemically reacts to release heat and gas [5], this can be military explosives, commercial explosives used by mining or blasting industries, or improvised explosives [6].

Since the beginning of the 20$^{th}$ century, one of the major concerns with security issues is the detection and identification of IEDs. In recent years there has been a rapid growth in IED terrorist attacks worldwide which include the Madrid train attacks in 2004 and the London bombings in 2005 [7], the Paris bombings in 2015 and most recently the Brussels bombings in 2016 [8]. These devices are mostly used in populated areas to distract, destroy, disrupt or delay daily operation of the state or opposition [9]. When employed in a populated area 90% of people injured in an IED explosion are usually civilians [10].

The Action on Armed Violence (AOAV) explosive monitor has recorded that since 2011 over 50% civilian deaths and injuries caused by explosive weapons have been victims of an IED device. In 2015 alone, the total number of casualties recorded was 43 786, of these 16 199 (48,64%) civilians were killed and injured by the use of IEDs [11]. The high rate of civilians injured emphasises the importance of increasing detection and identification techniques to intercept the IED before or after it is hidden and safely disarm the IED.

IEDs are built using a variety of materials which include metals, plastics, ceramics, and energetic materials. Each of these materials can further be divided into different constituents. The materials used in the construction of an IED are readily available to the public, relatively affordable, and without difficulty, the IED can be built [3,12].

Current detection methods used in the detection and identification of IEDs mainly involve bulk and trace detection methods. With trace detection methods, minute amounts of the energetic materials are detected in the form of vapour or particles. Trace technologies include electrochemistry, chemiluminescence, animal olfaction and ion mobility spectroscopy [13]. The aim of bulk detection is to detect macroscopic amounts of energetic materials. Bulk detection methods comprise of X-ray based, laser based, nuclear based and electromagnetic systems [14]. The challenges faced by these detection systems differ. Some systems result in false positive detection, wherein some systems the low atomic number (Z) materials give a similar shadow, and in other systems, the high-density materials hide underlying and overlying objects. Currently, there is no single method used to detect and identify a concealed energetic materials device. There is a need for a method that is quick and reliable. Detection methods that are currently employed in medical imaging may offer some capabilities in identifying these materials.

In radiological medical imaging, different X-ray energies and detection techniques are used to acquire an image depending on the study to be performed. The various modes of obtaining images are known as modalities [15]. For most imaging systems the peak kilovoltage ($kV_p$), tube current (mA), filtration and technique are varied according to the nature and size of the object to be detected and the image quality required. Each modality in its simplest form emits X-rays. Most medical imaging techniques use a system where the radiation is transmitted through an object, and the attenuation (absorption and scatter) is measured by a detector behind the object being imaged. This technique holds for all modalities even the ones with a moving detector such as computed tomography (CT) [16]. The detector provides intrinsic properties about the object such as material composition (density and Z number) and extrinsic parameters, which include the position and thickness of the object. The

advantage of using medical imaging modalities is that a wide range of energy levels can be utilised, from low kilovoltage (kV) energies to high penetrating megavoltage (MV) energies. This approach is investigated in this study to evaluate its potential to resolve the challenge of identifying a concealed energetic materials device.

## 1.2 Problem Statement

There are hundreds of IED base components available in thousands of combinations. IEDs do not have one form, which implies there are many ways to disarm one. The use of IEDs is a global threat and causes a devastating impact on the safety, stability, and development in communities [17]. Figure 1 is a flow diagram showing the step by step process an IED goes through, from the moment it is built, deployed, activated and the implications after that. An important measure in ensuring the IED is not activated is to intercept the IED before it is hidden during the deployment process.

Current methods used for detecting and identifying a concealed energetic materials device use X-rays. Identifying with confidence all the components of an IED is crucial as it helps safely defuse the threat. X-ray techniques which use low energies have difficulties in differentiating materials of low atomic number as they give the same contrast in a radiographic image [4,18].

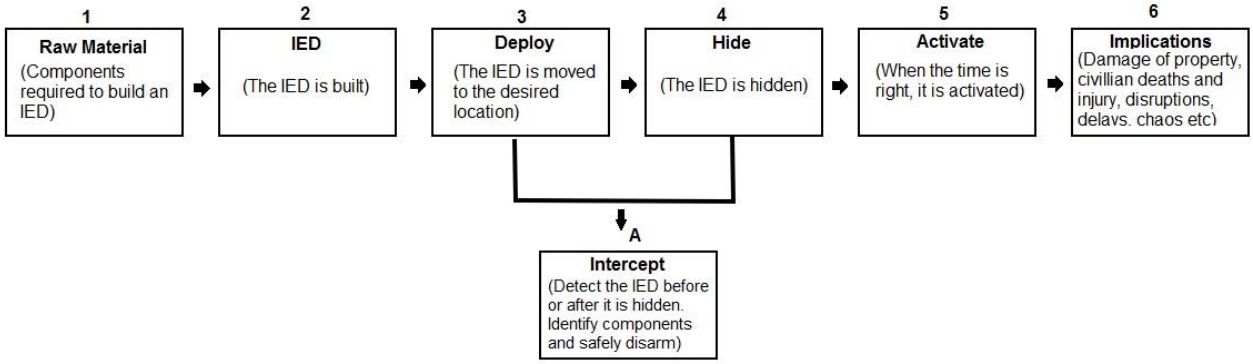



**Figure 1: A flow diagram showing the stages of the development and implications of an IED.**

## 1.3 Research aim

The purpose of this study was to determine which combination of medical imaging modalities and detector can enhance the identification of concealed energetic materials device.

## 1.4 General objectives

The overall objective of this study was to identify components of concealed energetic materials of an IED, with particular attention given to the identification of the detonator, using a range of medical imaging modalities. The objectives of this study included:

- Develop an inert (dummy) concealed IED free of active energetic materials for imaging.
  - Characterise the materials used to compose the device regarding its effective atomic number and material composition.
- Use different imaging modalities to resolve the materials inside the device with:

1. Low and medium energy X-ray sources (40 – 300 $kV_p$)
    - Standard diagnostic radiographic imaging using planar radiographic film and digital detection.
    - Reconstructed CT images using the Digital Imaging and Communications in Medicine (DICOM) standard, which is a standard used for handling and storing information images.
    - Kilovoltage therapy machine using radiographic and megavoltage film.
2. High energy X-ray sources (1 – 6 MV)
    - $^{60}Co$ teletherapy machine emitting 1.17 and 1.33 MeV gamma rays
    - Linear accelerator (Linac) producing a 6 MV bremsstrahlung photon beam.

# 2. LITERATURE REVIEW AND THEORETICAL FRAMEWORK

Black powder or gunpowder is the first known explosive. This energetic material contains both fuel and oxidizer. Explosives are unstable chemicals and mixtures that have the ability to explode with a certain range of degrees of violence [19]. The threat posed by IEDs is severe. They cause tremendous damage to property, injuries, and loss of life. Figure 2 shows a schematic diagram of the essential components of an IED.

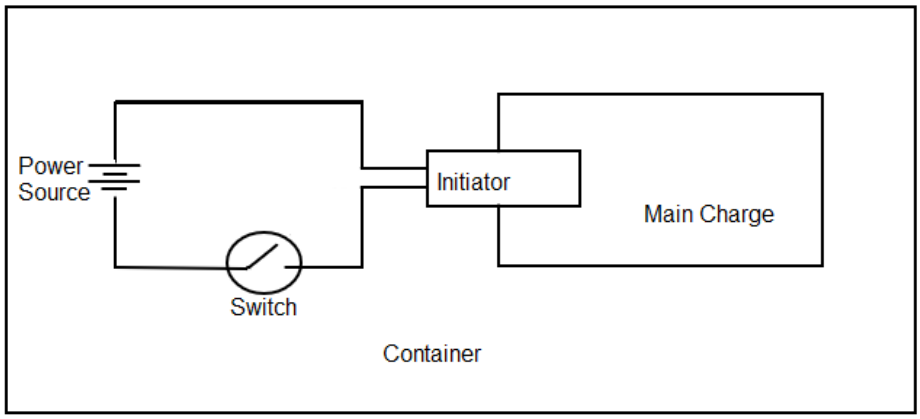



**Figure 2: A schematic diagram showing essential IED components.**

At its base, each IED may contain a power source, detonator/initiator, main charge, switch, container and shrapnel [6,20]. Most power sources either use a battery or charged capacitor to operate an electrical circuit, and circuit board. A typical material utilised in some batteries are alkaline, zinc-carbon, and lithium ion. The most common materials used in circuit boards include fibreglass with copper foil on either one or both sides of the circuit board. The circuit receives its command from the switch which, when turned on, activates the detonator. Various methods are used to trigger an IED using tilt switches (liquid metal mercury is used to open and close the circuit), tripwires (copper or metallic wires are used), and remote control (cell phones, remotes or walkie-talkies). An electric switch is used for control over the IED. The detonator is a device that is used to start a detonation. Figure 3 is a

schematic diagram of a commercial detonator. An electric detonator usually consists of a sensitive primary explosive mixture in a small rigid plastic container. The initiating explosive in the detonator is typically made of lead azide ($Pb(N_3)_2$) or lead styphnate ($C_6HN_30_8Pb$), which are high atomic number materials [21]. Electric detonators usually contain a base charge which is either Pentaerythritol tetranitrate (PETN) or Cyclotrimethylenetrinitramine (RDX) and varies with the manufacturer [22]. The detonator is initiated by an electric current which ignites an electric match situated in the detonator through the insulated lead wires, which are enclosed within the detonator.

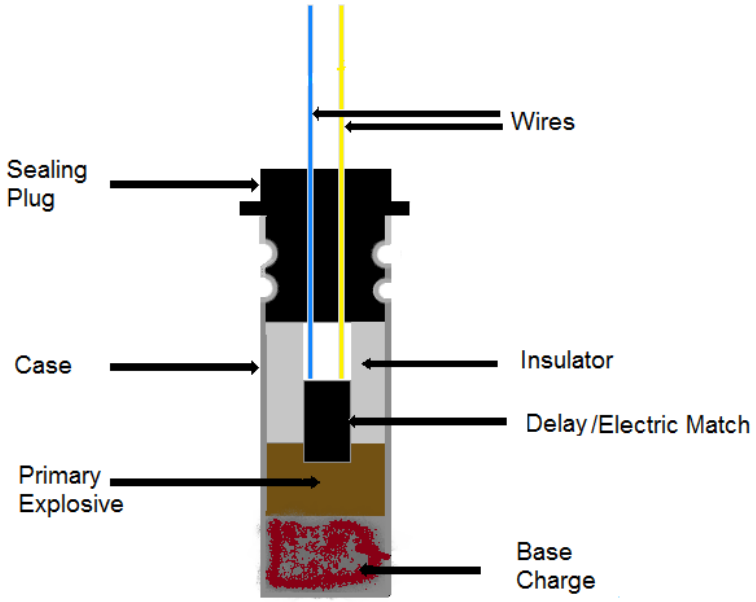



**Figure 3: A schematic diagram of a commercial electric detonator.**

The main charge is the component where the energy of the IED lies. This can be material from the military or commercial industries or improvised with common chemicals. The main charge is a secondary explosive which is insensitive to shock heat and friction. A detonator is required to initiate the blast. Most explosives contain elements such as carbon, hydrogen, nitrogen and oxygen (C, H, N, and O) and consist of densities in the range 1.2 – 2.0 $g/cm^3$ [23]. Shrapnel (ball bearings, nuts, nails, glass marbles, etc.) is used for expanding the range of the explosion so that it

is not only focused on the blast pressure alone and increases the severity and number of injuries and deaths. The container is the body where the IED components are kept; it provides concealment and transport for the IED. Typically the IED contains chemical mixtures, metallic compounds, organic and inorganic materials.

## 2.1 Explosives detection systems

Current techniques used to detect and identify explosive materials have some limitations which are discussed in this study. These limitations have stimulated the need to develop other methods for identifying IED materials [14]. The focus of this study is to identify macroscopic energetic materials (bulk detection method). Some bulk systems have been investigated by researchers which include: X-ray (photon) based, nuclear based, and laser based explosives detection [14]. These systems are discussed in this study.

### 2.1.1 X-ray interaction with matter

X-ray based explosives detection techniques for identifying explosive materials are used in public areas for security screening [4]. Different photon techniques are used to screen an object containing hidden materials. When photons interact with matter, they release electrons. For the energies of relevance to this study, photons interact with atoms in matter and produce electrons in three primary processes; the photoelectric effect, Compton effect, and pair production.

#### 2.1.1.1 Photoelectric effect

During the process of the photoelectric effect, all of the incident photon energy is absorbed by an atom; its energy is transferred to an atomic electron that is ejected [16]. The ejected electron is called a photoelectron. After the photoelectric interaction, the atom is ionised and there is a vacancy in the inner shell. A cascade of electron transitions occurs from higher to lower energy levels in order to fill the vacancy releasing characteristic X-rays or Auger electrons [24]. The photoelectric

effect occurs mostly when the energy of the incident photon is slightly greater or equal to the binding energy of the electron that is ejected.

The probability of the photoelectric effect is proportional to $Z^3/E^3$, where $Z$ is the atomic number of the material and $E$ is the incident photon energy. The photoelectric effect therefore dominates at low energies, and in high atomic number materials. At low photon energies the, attenuation is mainly governed by Z. This property is useful when imaging materials that have small variations in Z [25]. As the photon energy increases, the likelyhood of the photoelectric effect decreases and the Compton effect becomes more predominant [26]. The advantage of photoelectric effect is that there are no secondary scattered photons to degrade the image [24].

#### 2.1.1.2 Compton effect

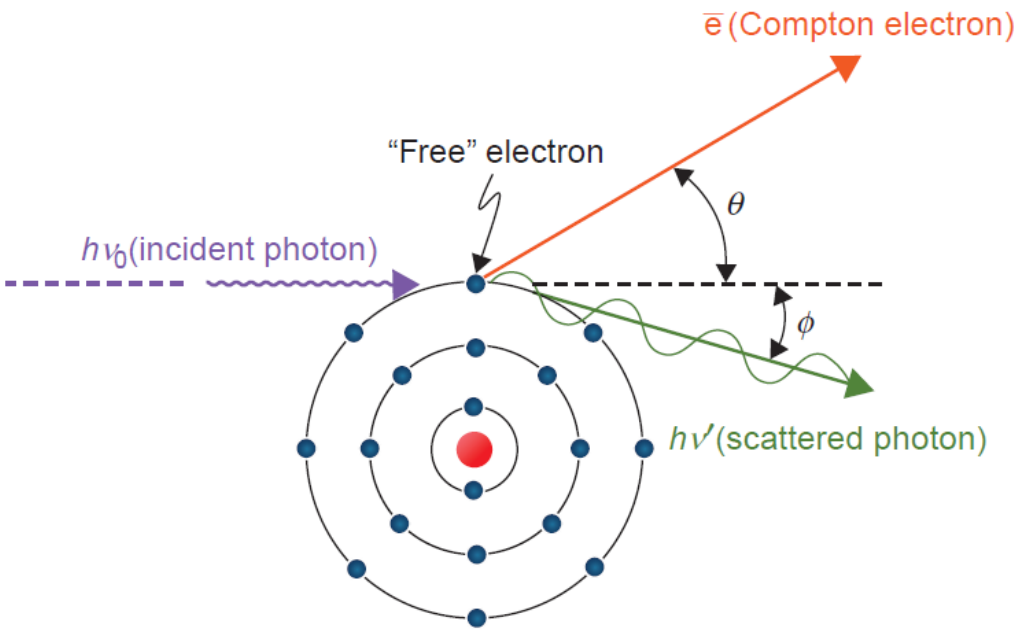



**Figure 4: An illustration of the Compton effect (from [27]).**

The Compton effect involves photon interaction with 'free' or valence shell electrons [16]. This occurs when the incident photon energy is much greater than the binding energy of the valence shell electron that is scattered. Figure 4 is a diagram showing

the geometry of the Compton effect. The photon loses some energy and is scattered at an angle $\phi$. The electron gains some energy from the photon and is emitted at an angle $\theta$ [25]. The ejected electron loses energy by ionisation and excitation of atoms in the surrounding material. The scattered photon may traverse the medium with or without further interaction in the medium [26]. Detection of scattered photons by the detector leads to a loss of radiographic contrast [24]. Because the Compton effect involves interaction with a 'free' electron, this makes it nearly independent of atomic number and dependent only on the amount of electrons per gram [27].

At high energies, the Compton effect decreases, and the pair production process becomes predominant. When the photon energy is greater than 1.02 MeV, the interaction with matter may result in pair production. The pair production process begins to dominate at much greater energies than the threshold energy of 1.02 MeV [27]. Pair production and other interactions relevant to very high energy photons have little relevance in this study and thus will not be detailed further.

### 2.1.2 Photon screening methods

Different photon screening methods are used to inspect concealed objects and include conventional transmission X-ray, Compton backscatter, dual energy X-ray and three-dimensional (3D) X-ray imaging.

#### 2.1.2.1 Conventional transmission explosives detection

Conventional X-ray techniques are widely used in airports for detection of contraband and explosives [14]. The fundamental principle applied when using X-ray transmission imaging involves transmitting a beam of X-rays through an object to a detector. A detector records modifications in the beam intensity due to attenuation of the X-ray beam penetrating the object. The transmitted intensity of a monoenergetic beam is attenuated exponentially [28]. The limitation of using this technique is that it provides integrated information of radiation transmissions, therefore, mixing properties of underlying and overlying material [29].

#### 2.1.2.2 Compton backscatter explosives detection

The Compton backscatter technique is a useful method which can be used to inspect concealed objects without the need for a transmission detector [14,30–32]. Backscatter imaging is a process whereby both the source and the detector are located on the same side of the object being imaged. This technique utilises scattered radiation generated by the Compton effect for imaging. Most of the backscatter applications use X-ray sources that produce Bremsstrahlung X-rays with a peak energy in the range of 50 $kV_p$ to 450 $kV_p$ [31].

In transmission imaging, the dark regions in the image indicate low-density materials. Compton backscatter imaging provides a complementary view. Compton backscatter is sensitive to low Z materials; this makes it useful for imaging explosives materials [28].

A practical advantage of using Compton backscatter is that it can image an object from one side without any contact or need for placing a detector behind the object being imaged [30]. A limitation to Compton backscatter is that since the energy of the scattered photons is low, they have a lower range and as a result, cannot penetrate materials deeply [28]. Typically, the energy of the scattered photons in the Compton backscatter is always less than the incident photon energy. No matter what the energy, for scattering in the fully backward direction the energy of the backscattered photon cannot exceed 255 keV [31].

#### 2.1.2.3 Dual energy explosives detection

Dual energy techniques are based on the principle of using both high and low energy X-rays for imaging enabling material discrimination. Various methods for collecting dual energy images are available including using multiple sensors with different spectral response, filtering the energy at the X-ray sensor and varying the input energy of the X-ray source [14]. Each energy level generates a different attenuation

coefficient with the higher energy levels giving information on electron density and the lower energy levels reflecting the effect of the atomic number [29]. The energy spectra are often broad, and the determination of the effective atomic number is only approximate. Materials are broadly characterised as organic (low Z) or inorganic and metals (high Z) [14,33].

#### 2.1.2.4 3D X-ray explosives detection

CT is one way of obtaining 3D information of a scanned object. The concept of CT is that the X-ray source and detector array simultaneously turn around ($360^0$) the object being imaged. Transmission images are acquired at multiple angular views (projections). CT solves the problem of overlying and underlying materials by applying mathematical algorithms to reconstruct slices of the object being imaged from the projection data. The radiation attenuation measurements of each slice are reconstructed to generate 3D images and volumetric views of the scanned object [14].

In medical imaging, artefacts are features that do not represent the actual structure of an object being imaged [34]. In medical CT streak artefacts occur when the attenuation levels in the object being scanned exceed the dynamic range of the detectors[15]. Usually, high Z materials cause streak artefacts in CT. In the security industry, CT is usually employed as a secondary investigation tool when suspicious materials are observed after scanning with a conventional planar system [33].

### 2.1.3 Nuclear technology based explosives detection

Nuclear technology based explosives detection techniques use neutrons instead of photons. Fast neutrons are produced by a radioisotope or a neutron generator. Neutrons are not affected by electromagnetic forces and therefore interact with all nuclei [29,35]. When the neutrons are emitted from the source, they are captured by the atomic nuclei, and gamma rays are emitted from the radioactive decay of the

atomic nuclei [36]. The gamma rays could have high penetrating power, which varies with the type of nuclear reaction, thus allowing detection of bulk materials [37].

The irradiated object is surrounded by an array of scintillation detectors. The detectors are shielded from direct exposure from the neutron source [33]. The main nuclear physics based techniques used for explosives detection include fast neutron analysis; thermal neutron analysis; pulsed fast thermal neutron analysis; and pulsed fast neutron analysis. Neutron-based techniques are not yet accepted in the security industry because of cost, shielding and implementation difficulties compared to photon detection [23].

### 2.1.4 Laser based explosives detection

A laser-based technique involves scanning the surface of an object and analysing the resulting light. This method uses laser-generated infrared radiation [14]. When the radiation interacts with the explosive residue, it will initiate microbursts. These bursts can be detected and generate light which can be used to identify the characteristics of the hidden explosive [38]. This technique offers the possibility of near real-time detection of explosives. A disadvantage is that this system only screens for residue on the surface of the object.

## 2.2 Theoretical framework of imaging

### 2.2.1 Film

Radiographic film is one of the most used methods of detection in hospitals. In medical physics, film is not only used for clinical imaging, but it also has a broad variety of applications which include verifying patient position [39], small field dosimetry [40], and quality assurance (QA) of intensity modulated radiation therapy [41].

The basic composition of film has remained the same over the years consisting of a base, emulsion (gelatin + grain) and protective coating. Figure 5 shows a schematic diagram of radiographic film. The base is transparent allowing light to be transmitted. The polyester base is covered with emulsion either on one side or both sides. The emulsion consists of silver halide crystal grains which are surrounded by gelatin. Gelatin holds the grains together and protects the unexposed grains from reduction during development [40]. The composition of the emulsion determines the basic sensitivity of the film. High sensitivity films have a larger grain size and require less exposure to create an image than low sensitivity films, which contain submicron grain size [40].

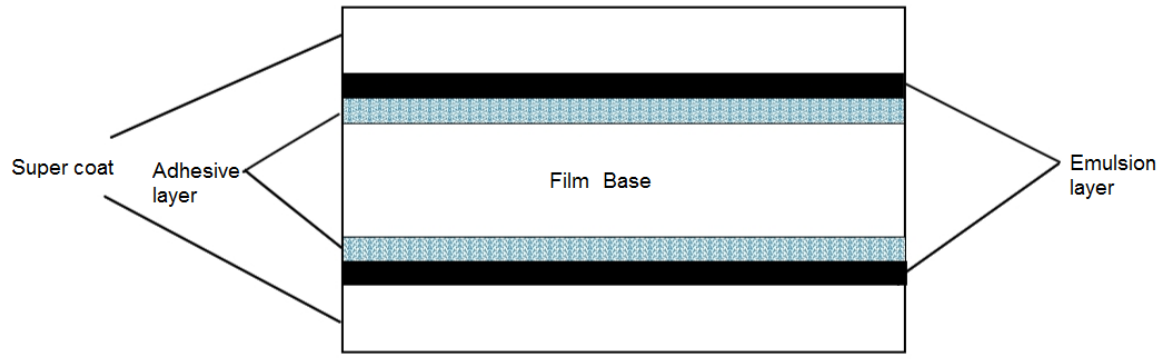



**Figure 5: A diagram showing the cross-section of radiographic film.**

When film is exposed to ionizing radiation, the interaction between the ionizing radiation and the silver halide crystals produces a latent image. The non-irradiated grains remain inactive. The combination of the irradiated and non-irradiated grains forms the latent image. The film is processed in a dark room using a chemical developer. Processing includes developing, fixing, washing and drying the film.

Film-screens are used to increase the sensitivity of a film. Double emulsion film is placed in between two intensifying screens and enclosed with a protective cassette. When the X-rays strike the intensifying screen, the radiation is absorbed by the

fluorescent screen and emitted as visible light which then interacts with the emulsion in the film, and an image is formed. The film is then developed in a darkroom using chemicals [42].

Radiochromic film contains an active layer and a yellow marker dye. The yellow dye darkens when irradiated, the colour change in the film can be noticed immediately, but the reaction process continues for at least 8 hours [41]. This film is insensitive to visible light, and the film is self-developing as it undergoes polymerization.

### 2.2.2 Digital detectors

Digital radiography systems convert the energy of X-ray photons into electrical signals which are then digitized. Digital radiography systems consist of solid state, flat panel, and large area detectors. In general, digital detectors have two configurations, direct conversion system and indirect conversion system [26].

Direct conversion systems use a photoconductor to convert X-rays directly into an electric signal. Various materials are used to construct photoconductors these may include amorphous selenium, lead iodide, and cadmium zinc telluride [25].

Indirect conversion systems use a scintillation material to first convert the energy of the X-ray into visible light, the light is then converted into electrical signals. Scintillating materials used include amorphous silicon and cesium iodide [25].

An electronic portal imaging device (EPID) is mounted on a linear accelerator, this device uses electronic image acquisition and contains an amorphous silicon detector [43]. In medical imaging, EPIDs are used for patient positioning, QA tests and dosimetry verification [44]. An EPID phantom is used for routine tests on linear accelerators for image quality, geometric accuracy and operational safety [45].

### 2.2.3 Image quality

The interaction between the transmitted radiation through the object of interest and the difference in attenuation properties in the object is what gives the distinct detail in a particular image as a function of beam quality. Image quality is determined by the type of imaging method used which depends on the type of source, and detector combination used [46]. In some cases, the spatial resolution might be a priority, and in other instances, the contrast might be a priority.

#### 2.2.3.1 Contrast and resolution

Contrast refers to the difference in signal intensity (grey scale) on an image. An image with uniform grey scale has no contrast, and an image with transitions between dark grey and light grey areas has high contrast. Spatial resolution describes the amount of detail that is visible on an image. This relates to the ability of an imaging system to distinguish detail and to display two unique objects closely separated in space [16]. An imaging system demonstrating the presence of small objects in an image has a high spatial resolution [15].

#### 2.2.3.2 X-ray tube operation

X-ray tubes are operated at high voltages. The energy of the photons produced by an X-ray tube depends on the energy of the electrons bombarding the target of an X-ray tube. An increase in $kV_p$ increases the efficiency of X-ray production. The $kV_p$ controls the penetrating power of the X-ray beam and affects the resulting radiographic contrast.

The product of tube current (milliampere) and exposure time (seconds), milliampere-seconds (mAs), determines the number of electrons bombarding the target of an X-ray tube. The mAs governs the amount of X-rays reaching the detector. As tube current increases the intensity of X-rays also increases. Applying low mAs may result in an underexposed film. The distance from the source to the detector affects the radiation intensity by the inverse square law.

#### 2.2.3.3 Film processing

Film processing also affects the quality of the image. Poor image quality can be caused by the poor quality of a dark room. The dark room should be light, chemical, dust and moisture free [40]. The processor temperature and chemicals must be controlled, and the system should be maintained regularly. All the images were digitised and processed using software.

# 3. METHODOLOGY

An inert dummy IED was built at the Council for Scientific and Industrial Research (CSIR) and is shown in Figure 6. The dummy IED was in the form of a briefcase and had dimensions of 43 cm x 32 cm x 16 cm (Width (W) x Length (L) x Height (H)). The briefcase was marked at the centre to maintain a constant imaging position relative to the source and geometry of the machine. The materials which were used in this study including their effective atomic number, material composition and approximate weight are listed in Table 1.



**Figure 6: An image of the dummy IED built at the CSIR.**

**Table 1: A table showing the effective atomic number of materials used in the briefcase.**

| Physical Properties | Materials | Material Composition | Approximate weight (g) |
|---|---|---|---|
| $Z_{eff}$ < 10 | Electric detonator | Pb azide/ Pb styphnate | - |
| $Z_{eff}$ = 10 – 15 | Putty | Calcium carbonate and linseed oil | 1000 |
| | Switches | Plastic, steel, copper | - |
| | Circuit board | Fibreglass, copper | - |
| | Cell phone | Plastic, circuit | 164 |
| $Z_{eff}$ > 15 | Nails | Steel | 1.39 |
| | Conducting wires | Copper | - |
| | Batteries | Alkaline/ Carbon zinc | 45 |

An Electronic Portal Imaging Device (EPID) Quality Control (QC) phantom of outer dimensions of 25 cm x 25 cm x 4.2 cm was used as a standardised measure of image quality at all modalities. The EPID QC phantom contains different materials which include copper step wedges (Z=19), an aluminium block (Z=13), square brass (alloy material with a mixture of copper and zinc (Z=30)) blocks and a brass modulation transfer function (MTF) [47]. Most of the materials used in the EPID phantom are of high Z. The phantom has known medical qualities and some materials in the phantom have similar properties to materials used to build an IED. An image of the EPID QC phantom is shown in Figure 7.

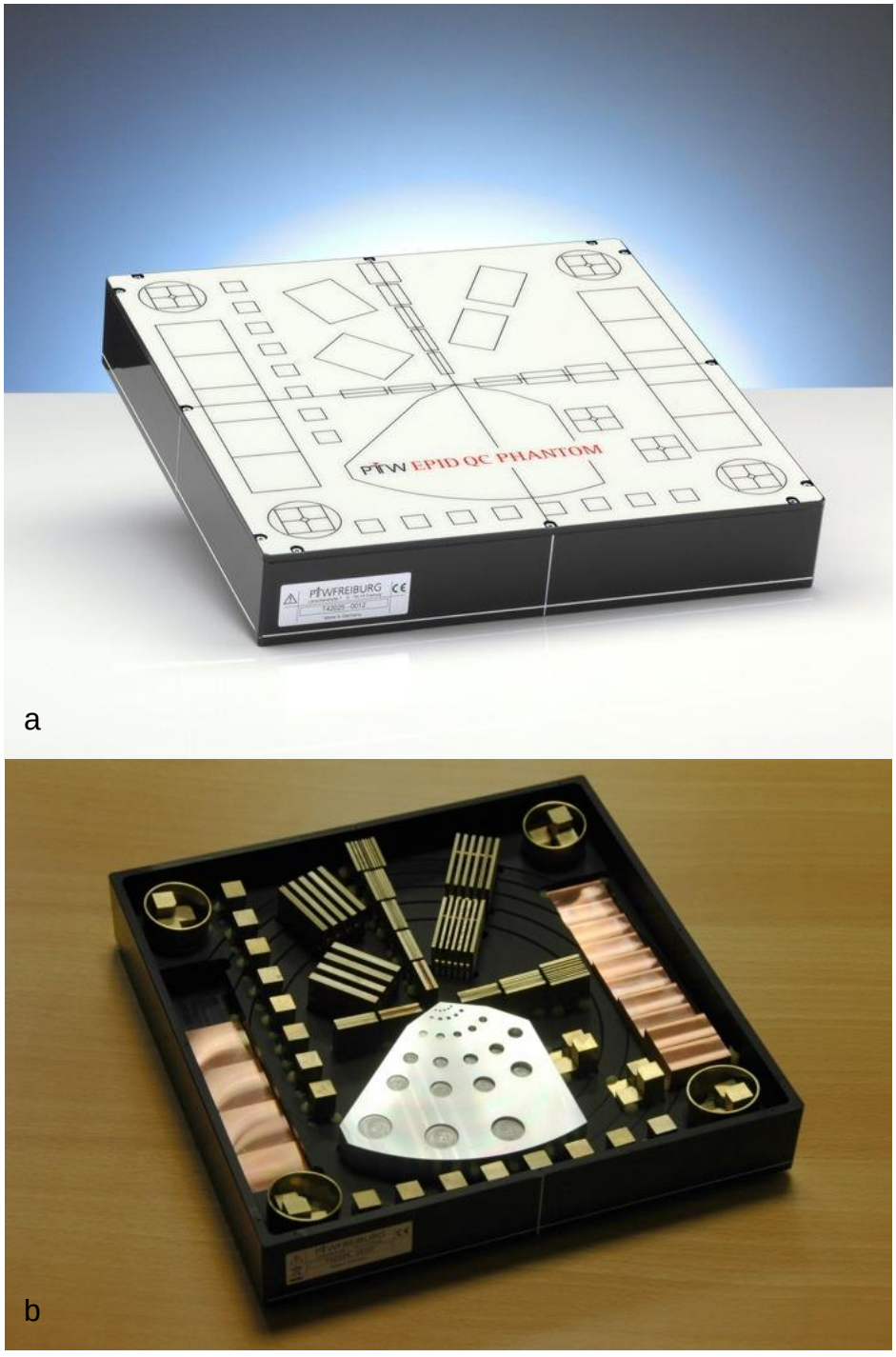



**Figure 7: a) An image of the PTW EPID QC phantom (from [45]); b) the materials inside the EPID QC phantom (from [48]).**

Three different types of film were used for this study, namely Fuji medical X-ray film (radiographic), Kodak X-Omat V ready pack film (radiographic) and Gafchromic EBT2 (radiochromic) film.

The Fuji medical X-ray radiographic film of dimensions of 35 cm x 43 cm was placed in between two intensifying screens and enclosed with a protective cassette. This is high sensitivity film and required very low exposures.

The Kodak X-Omat V ready pack radiographic film of dimensions of 25.4 cm x 30.5 cm was contained in a sealed envelope. The film was used in direct exposure mode. This is low sensitivity film and requires high exposures to generate a latent image. The film has an optimum dose of 50 cGy [40,49].

The radiographic film was taken from a single batch and was processed using a single Konica Medical Film Processor SRX-101A in order to ensure consistent imaging results.

The Gafchromic EBT2 film of dimensions 35.6 cm x 43.2, radiochromic film is preferably used with high energies. The film can be used up to approximately 8 Gy using the dye marker feature and can be used to measure up to at least 50 Gy without the dye marker feature [50].

The advantage of using film is that a permanent record of high spatial resolution is obtained. All films were scanned using an Epson 10000 XL flatbed scanner, in order to obtain the digital format of the films. The digital image obtained was saved in tagged image file format (.tiff). The analysis of all the collected data from the different imaging modalities was done using PTW VeriSoft software. This enabled the same image manipulation and processing as is used for direct digital imaging.

Digital images were acquired from the CT and EPID and were stored using the DICOM standard.

## 3.1 Modalities

Figure 8 shows the Toshiba LX 40 medical simulator and Figure 9 is a schematic diagram of the setup used in this study. The Toshiba medical simulator uses an X-ray tube as its source of radiation. The X-ray source delivers X-ray energies in the range from 20 $kV_p$ to 150 $kV_p$. For this study, an energy range from 40 $kV_p$ to 95 $kV_p$ was used, and the tube current (mA) was varied in order to obtain the same exposure on the film. Since low energies were used here, the method of detection used for this modality was the Fuji medical X-ray film which was enclosed in a light tight cassette. A radiation field size that covered the entire object was selected. The source to surface distance (SSD) was kept at 100 cm for all imaging. The object was placed on the image intensifier (II) with the film directly underneath the object, to minimise magnification and optimise resolution of the object being imaged. Three different energies were selected at this modality: 95 $kV_p$ with 10 mAs, 60 $kV_p$ with 27.5 mAs, and 40 $kV_p$ with 10 mAs, the half value layer (HVL) of each energy was 4.33 mm Al, 2.71 mm Al, and 1.91 mm Al respectively.

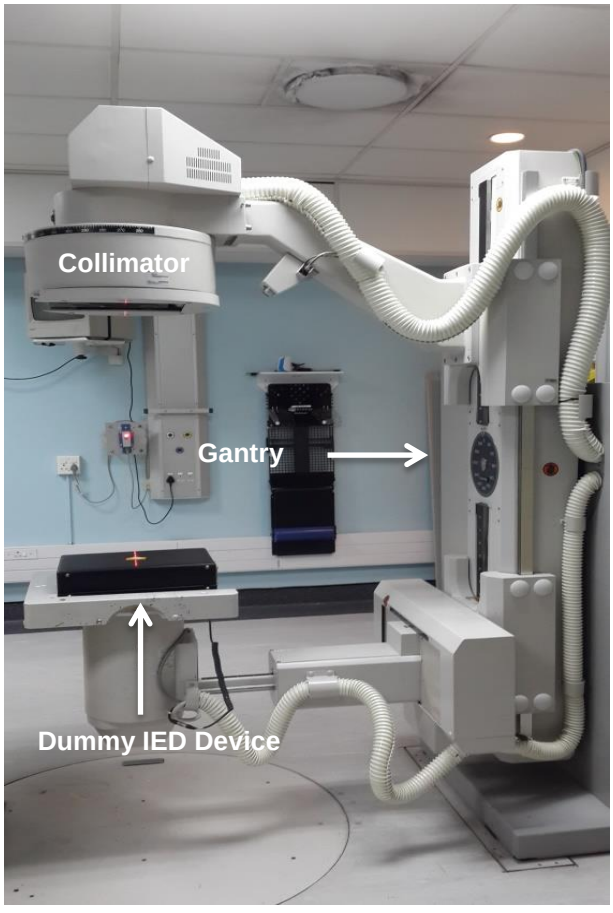



**Figure 8: An image of the Toshiba medical simulator.**

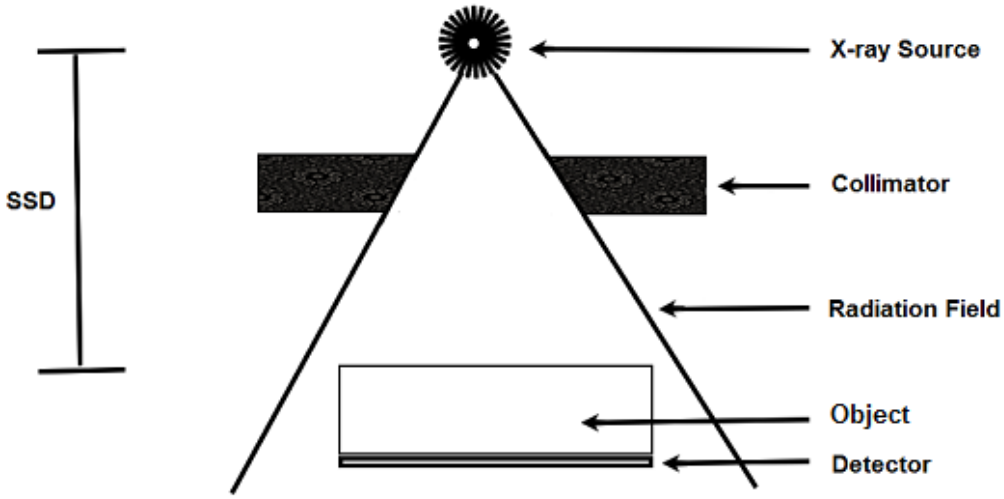



**Figure 9: A schematic diagram of the Toshiba medical simulator setup used for imaging the briefcase and phantom.**

A Siemens Primus Linac was used in this study. Figure 10 is a schematic diagram of a medical Linac. The Linac, used in radiation therapy, uses very high-frequency microwaves to accelerate electrons to high energies as used for this study. Pulsed microwaves are produced in a magnetron or klystron with a frequency of about 3000 MHz per pulse. The microwaves are driven through a waveguide system and are injected into an evacuated accelerator tube and simultaneously an electron gun produces electrons that are injected into the accelerator tube [27]. The electrons are accelerated and hit a target to produce X-rays.

The Linac has a built-in digital imaging device called an EPID which is used to acquire digital images. The object was placed on the treatment bed with the EPID positioned under the bed in line with the object being imaged. An X-ray beam with a nominal energy of 6 MV was selected and 3 MU (monitor units) were delivered. The set field size on the Linac was 26 cm x 26 cm. The EPID QC phantom was imaged at a SSD of 96.2 cm. The briefcase was imaged at a SID of 130 cm. The images were stored using the DICOM standard.

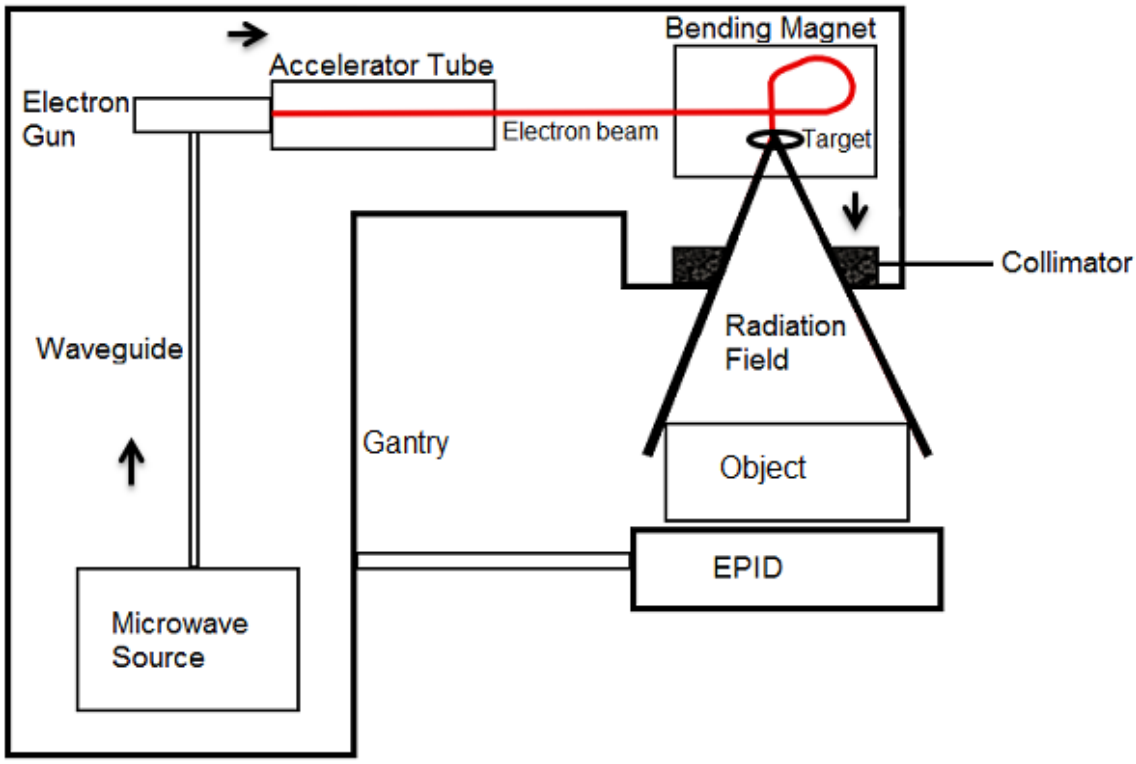



**Figure 10: A block diagram of a typical medical linear accelerator with an EPID, showing the setup used for imaging the briefcase and phantom.**

Figure 11 is an image of the MDS Nordion Equinox $^{60}$Co teletherapy machine, and Figure 12 is a functional diagram of the setup. The radioactive source used is sealed in a stainless steel capsule situated in the head of the machine which is heavily shielded with lead [27]. The source is pneumatically driven from the shielded position to a fully exposed position during the delivery of radiation.




**Figure 11: An image of the $^{60}$Co teletherapy machine.**

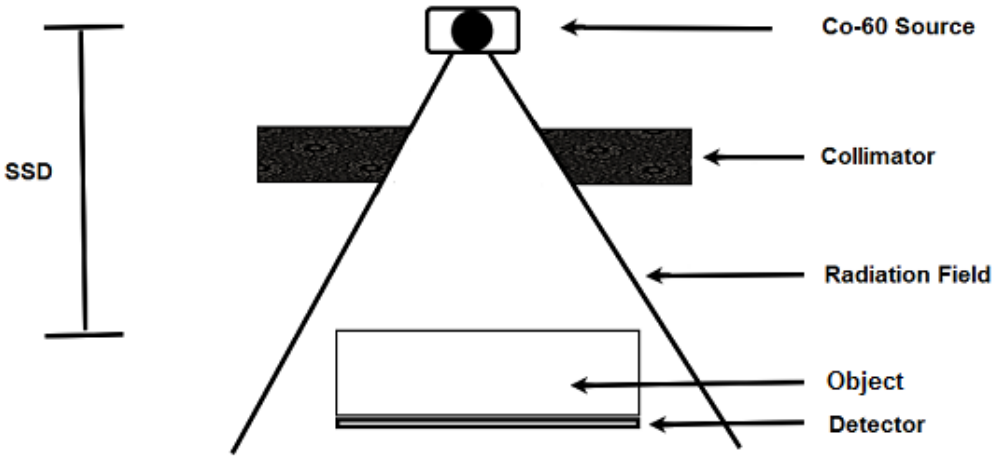



**Figure 12: A schematic diagram of the imaging setup on the $^{60}$Co teletherapy machine.**

The source emits photon energies of 1.17 and 1.33 MeV. The object was placed on the bed with the detector directly underneath the object being imaged. Three modes of detection were used: Fuji film, Kodak film, and Gafchromic film. The position of the gantry relative to the object being imaged was varied in order to obtain different projections. Table 2 shows the different setups used. The field size was opened to cover the objects being imaged.

**Table 2: The exposure time and scanning position of each film used in the study.**

| Film | Gantry position | Exposure time (min) Briefcase | Exposure time (min) EPID Phantom |
|---|---|---|---|
| **Fuji** | Flat ($0^o$) | 0.03 | 0.02 |
| | $270^o$ | 0.04 | - |
| **Kodak** | Flat ($0^o$) | 1.2 | 0.29 |
| | Side view ($270^o$) | 1.2 | - |
| **Gafchromic** | Flat ($0^o$) | 24 | - |

Figure 13 shows a schematic diagram of the GE HiSpeed CT machine. The X-ray tube and detector array rotate around the object being imaged, obtaining different projections of the object. The object was placed at the centre of the machine bore. A scout image of the object was obtained to select the region of interest. The CT scanner was operated at 120 $kV_p$ with a tube current of 120 mA and a slice thickness of 5 mm. The images were stored using the DICOM standard.

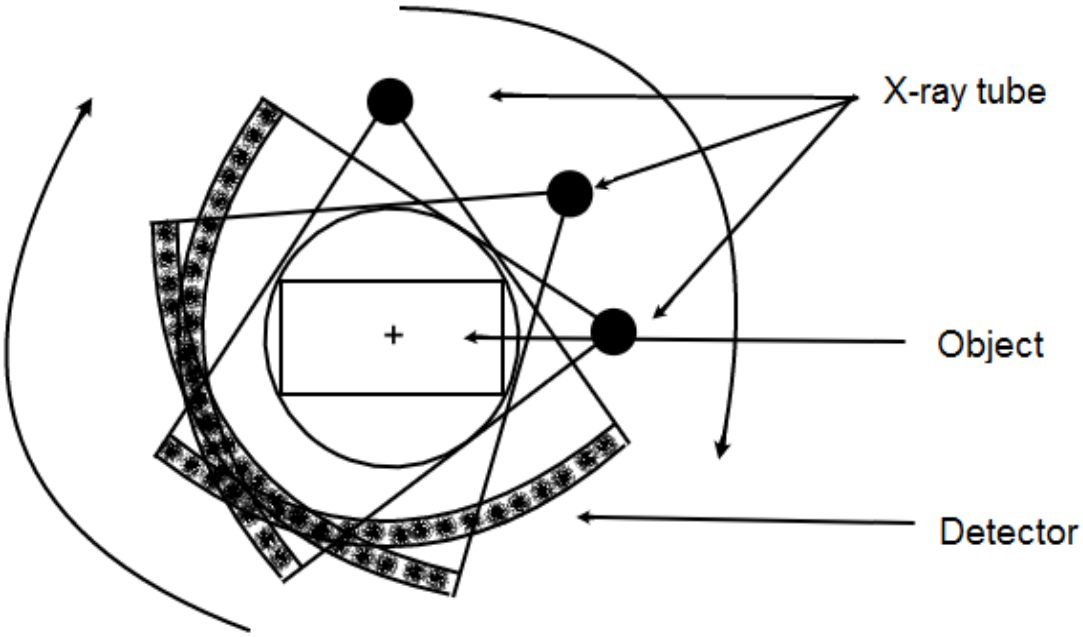



**Figure 13: A schematic diagram of a CT scanner showing the X-ray tube and detector arrays rotate around the object being imaged.**

The Gulmay Medical Ltd D3300 orthovoltage teletherapy machine uses an X-ray tube and produces X-ray potentials in the range of 95 $kV_p$ to 300 $kV_p$. Figure 14 shows a schematic diagram of the imaging process using the orthovoltage teletherapy machine. Different filters are used to achieve different beam qualities. In this study, 95 $kV_p$, 180 $kV_p$, and 280 $kV_p$ with HVL 3 mm Al, 1 mm Cu and 3 mm Cu respectively were used. The tube currents were 15 mA, 10 mA, and 8 mA respectively.

An applicator placed in the head of the treatment machine was used to collimate the beam to 20 cm x 20 cm, at a source to collimator distance of 50 cm, the largest available at Charlotte Maxeke Johannesburg Academic Hospital (CMJAH). The dimensions of both the EPID phantom and briefcase were bigger than the applicator. The endface of the applicator was therefore not placed on the surface of the irradiated object. Since the radiation beam is divergent, the head of the machine was raised such that the radiation field covered the object being imaged. The mode of

detection used was the Kodak X-Omat V (ready pack) film. The film was placed directly under the device being imaged.

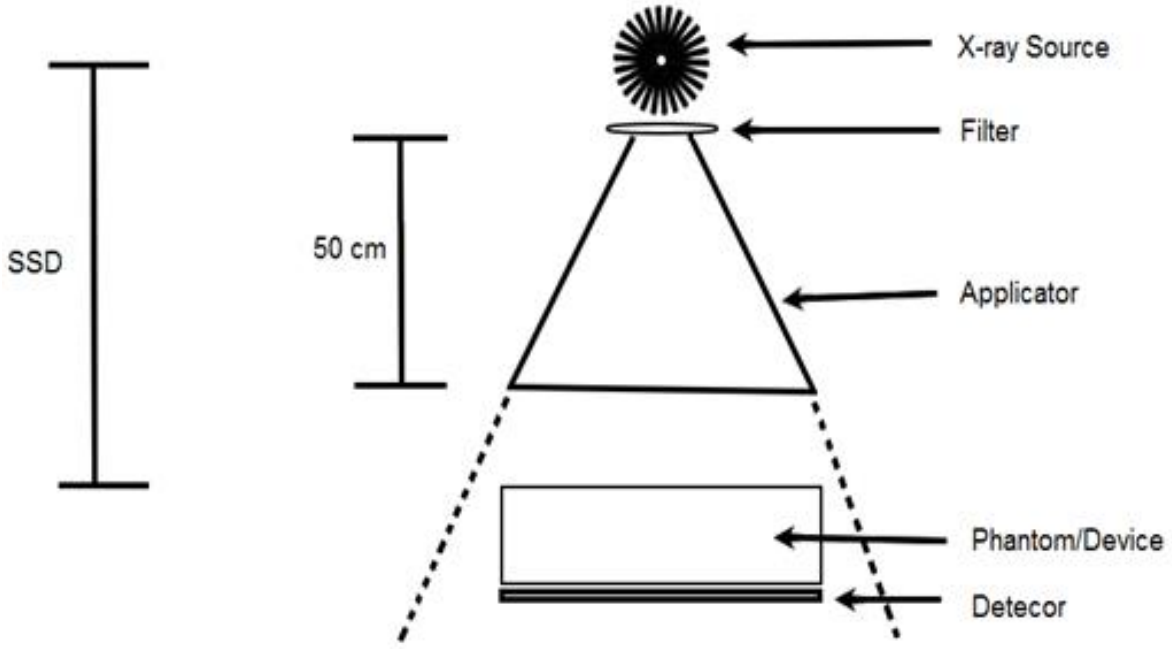



**Figure 14: A schematic diagram of the setup used to image the phantom and the briefcase on the orthovoltage teletherapy machine.**

## 3.2 Summary of experimental procedure

A summary of the modality/detector combinations used for this study is provided in Table 3.

**Table 3: Summary of the experimental procedures used in this study.**

| Modality | Delivered Energy | Detector |
|---|---|---|
| **Toshiba medical simulator** | 40 $kV_p$, 10 mAs; 60 $kV_p$, 27.5 mAs; 95 $kV_p$, 10 mAs | Fuji film |
| **CT scanner** | 120 $kV_p$, 120 mA | Digital detector array |
| **Orthovoltage teletherapy machine** | 95 $kV_p$; 180 $kV_p$; 300 $kV_p$ | Kodak film |
| **$^{60}$Co teletherapy machine** | 1,17 MeV & 1,32 MeV | Fuji film |
| | | Kodak film |
| | | Gafchromic film |
| **Linac** | 6 MV | EPID |

# 4. RESULTS AND DISCUSSION

## 4.1 EPID QC phantom imaging

The results from imaging the EPID QC phantom at the different medical imaging modalities are presented below. The source and detector combination which provided the best image quality (contrast and resolution) of the EPID QC phantom was selected in each modality to image the briefcase.

### Medical simulator

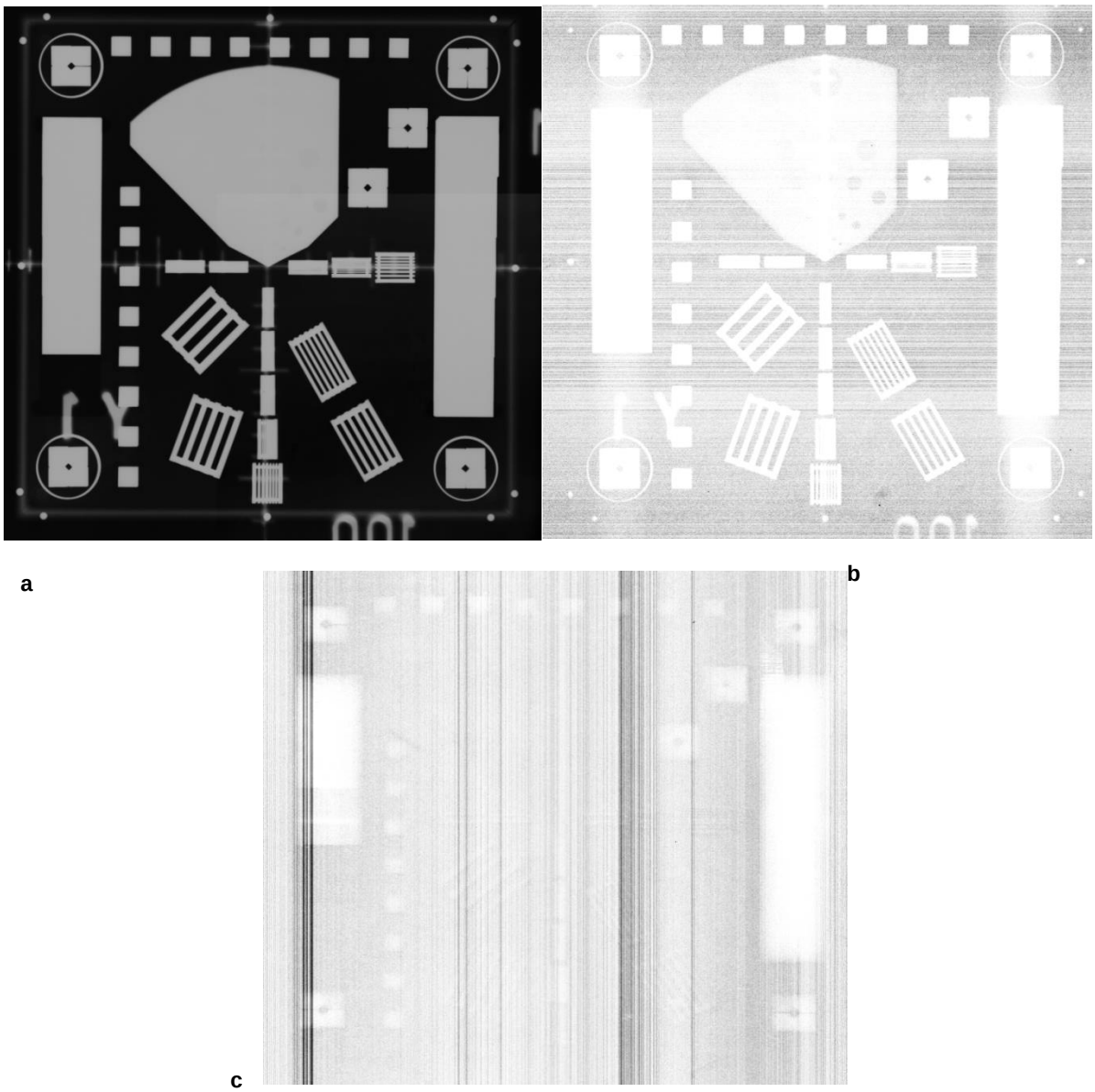
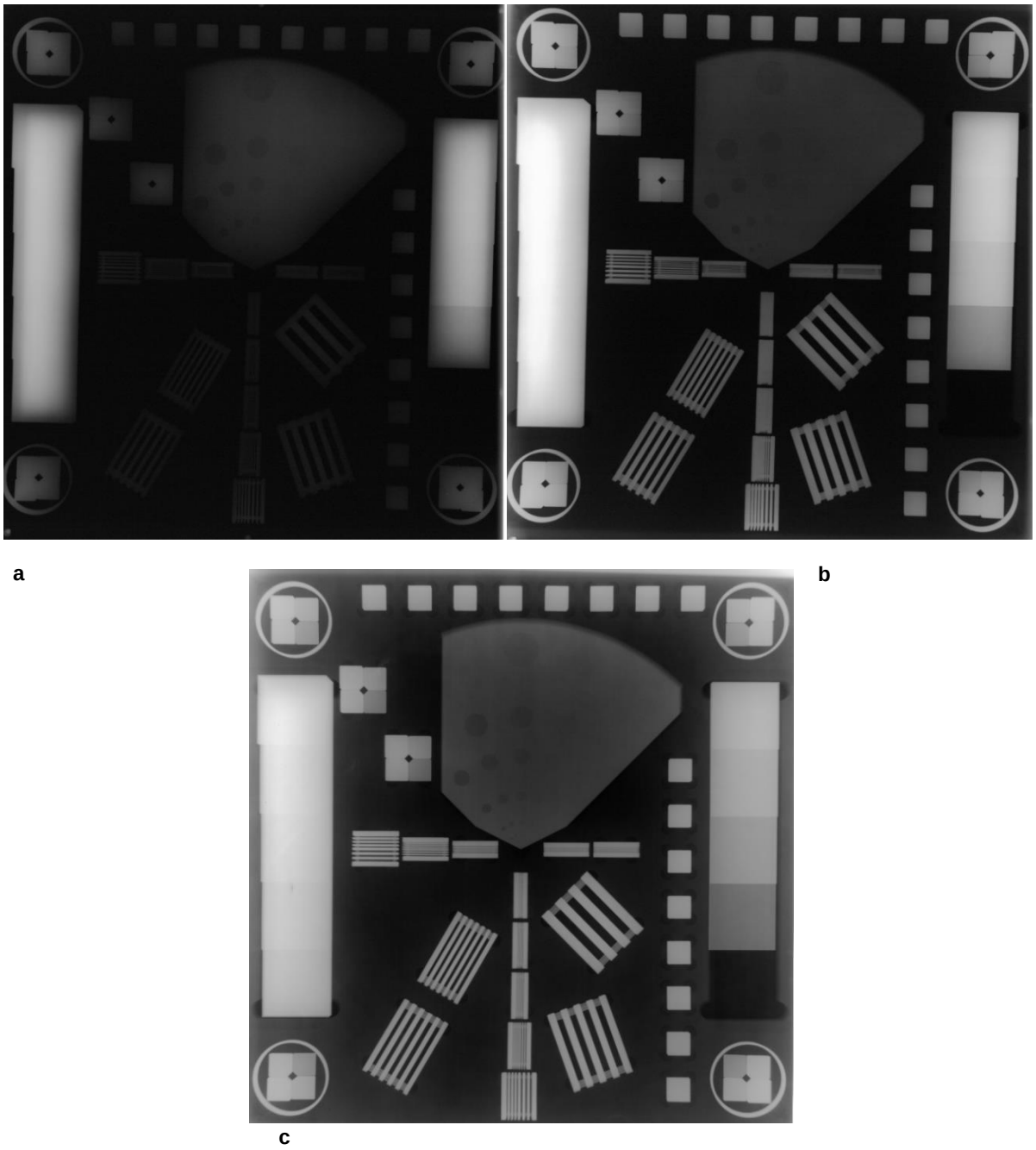



**Figure 15: Images of the EPID phantom at the Toshiba medical simulator using Fuji film. The energy and tube current were: a) 40 $kV_p$, 10 mAs; b) 60 $kV_p$, 27.5 mAs, and c) 95 $kV_p$, 10mAs.**

The Toshiba medical simulator displayed the dominance of photoelectric absorption at low energies and high Z since the photoelectric effect is proportional to $Z^3/E^3$. Figure 15 (a), had the highest contrast and was selected to image the briefcase.

## Orthovoltage



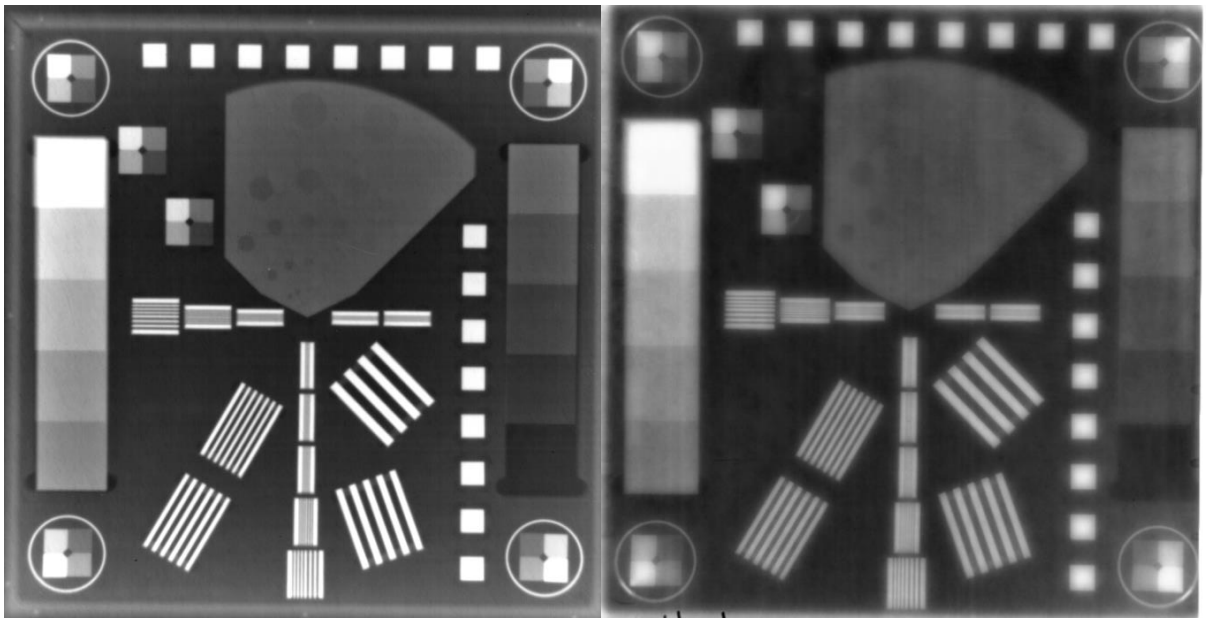
**a** **b**

**c**

**Figure 16: Images of the EPID phantom radiated at the orthovoltage teletherapy machine using a) 95 $kV_p$, b) 180 $kV_p$ and c) 300 $kV_p$ with Kodak oncology film as a detector.**

The MTF brass blocks, used for resolution testing, were most visible at 300 $kV_p$. The contrast was also good and the the Cu step wedges could be seen.

### Cobalt-60



a b

**Figure 17: Images of the EPID phantom radiated using the $^{60}Co$ teletherapy machine with a) an exposure time of 0.02 min using Fuji film and b) an exposure time of 0.29 min using the Kodak oncology film.**

The $^{60}Co$ teletherapy machine produced a good quality image of the EPID phantom, The Fuji film was selected to image the briefcase since it had a better resolution than the Kodak oncology film.

**Linear accelerator**

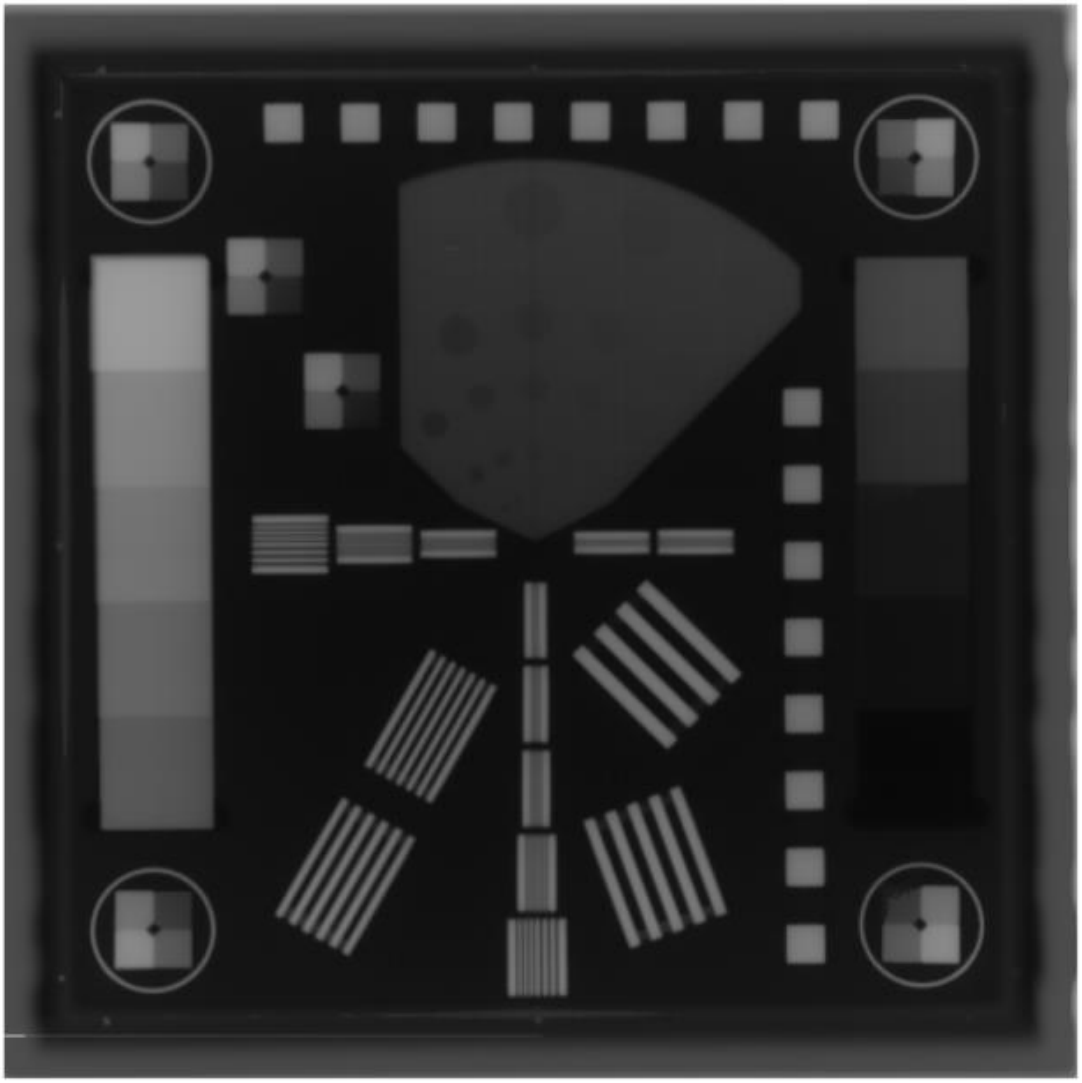


**Figure 18: An image of the EPID QC phantom using 6 MV, delivering 2 MU at the Linac using the EPID as a detector.**

The EPID QC phantom is designed for use at 6 MV with the EPID imager. As a result, the image quality at this modality using the EPID phantom was good, with good resolution and contrast. All the copper step wedges were visible, the holes on the aluminium block could be seen, and the MTF blocks could be distinguished.

## 4.2 Briefcase imaging

### 4.2.1 Radiotherapy simulator imaging

Figure 19 shows the resultant image of the briefcase taken using the Toshiba medical simulator at 40 $kV_p$ and 10 mAs on the Fuji medical X-ray film. Table 4 lists the materials observable using the medical simulator. The contrast on the film was high. As a result, there was very little grey scale displayed on the film, the image was basically dark grey, and other areas light grey.

Small materials present on the circuit board and cell phone were not clearly visible hence low spatial resolution was displayed on the film. Underlying and overlying materials could not be seen at this modality because this was a planar image. Underneath the putty, there were more nails which are not visible as the putty absorbed the radiation energy. The low energy radiation beam delivered on the briefcase was absorbed by the materials, an indication of the predominance of the photoelectric effect. This modality would be ideal for imaging low atomic number materials, allowing more beam transmission from the irradiated object.

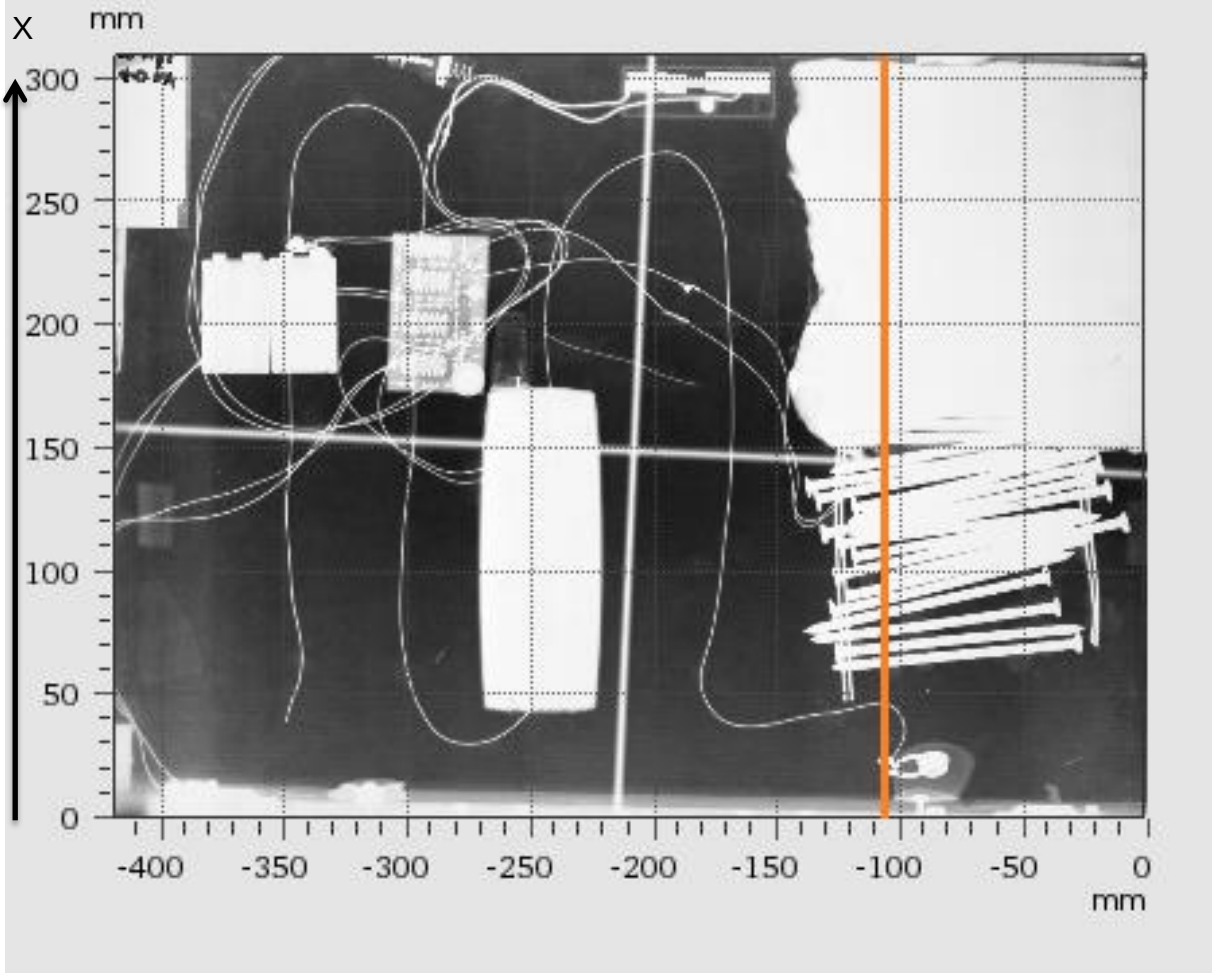



**Figure 19: An image from the Toshiba medical simulator with energy and tube current at 40 $kV_p$ and 10 mAs respectively, using Fuji film as a detector.**

**Table 4: Materials observed using the Toshiba medical simulator.**

| Items | Visible | Comment |
|---|---|---|
| Putty | Yes | |
| Nails | Not all | Some nails were hidden under the putty |
| Wires | Yes | Trip wires were masked by the putty |
| Cell phone | Yes | Components inside the phone were not visible |
| Circuit board | Yes | The elements on the board were not visible |
| Battery | Yes | The cylindrical cells in the battery could not be seen |

| | | |
|---|---|---|
| Underlying/overlying material | No | Low energy could not penetrate deeply into materials |
| Switches | Yes | |
| Detonator | No | The nails masked the detonator |

The orange line on the image in Figure 19 shows where data were collected from the film for further analysis, and these data are displayed on the graph in Figure 20. The position of the orange line in the image is approximately the same for all subsequent images of the briefcase. The position of the line was selected to coincide with the position of the dummy detonator in the briefcase. The arrow in Figure 19 and Figure 20 relate the image to the x-axis in Figure 20. In Figure 19 the y-axis is a relative measure of the optical transmission along the orange line. The graph was obtained using the PTW VeriSoft software.

The peaks on Figure 20 show high optical transmission. The nails and the putty are not distinguishable.

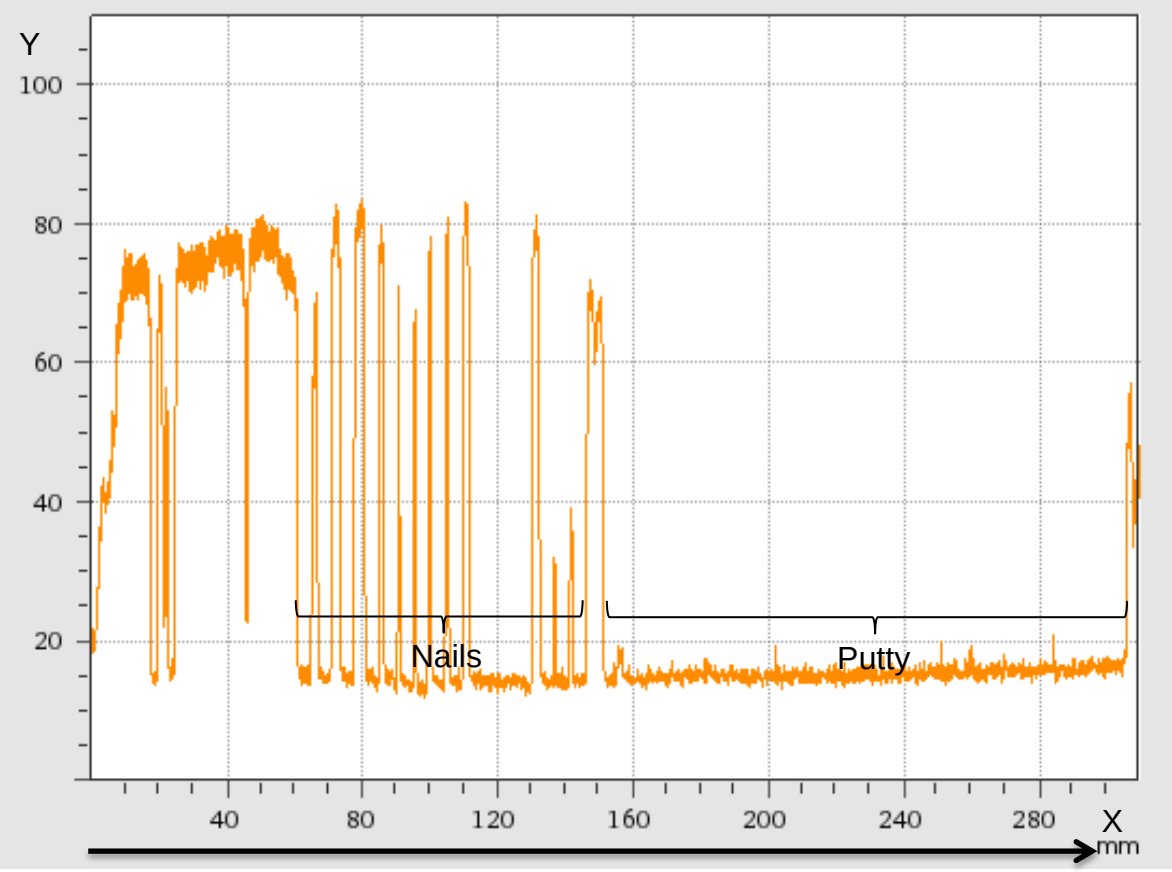



**Figure 20: A graph showing optical transmission collected from the Fuji film using the Toshiba medical simulator.**

### 4.2.2 Linear accelerator

Figure 21 shows a Linac EPID image of one-half of the briefcase (with putty). The entire briefcase could not be scanned at once since the field size of the imager was smaller than the dimensions of the briefcase. Most materials were not visible (wires, switches, and detonator) using this modality, Table 5 lists these materials. Underlying and overlying materials could be seen at this modality, the high penetrating power of the beam at this modality made it possible. The digital image was dark with high contrast and low spatial resolution; the high Z number and dense materials were distinctly visible.

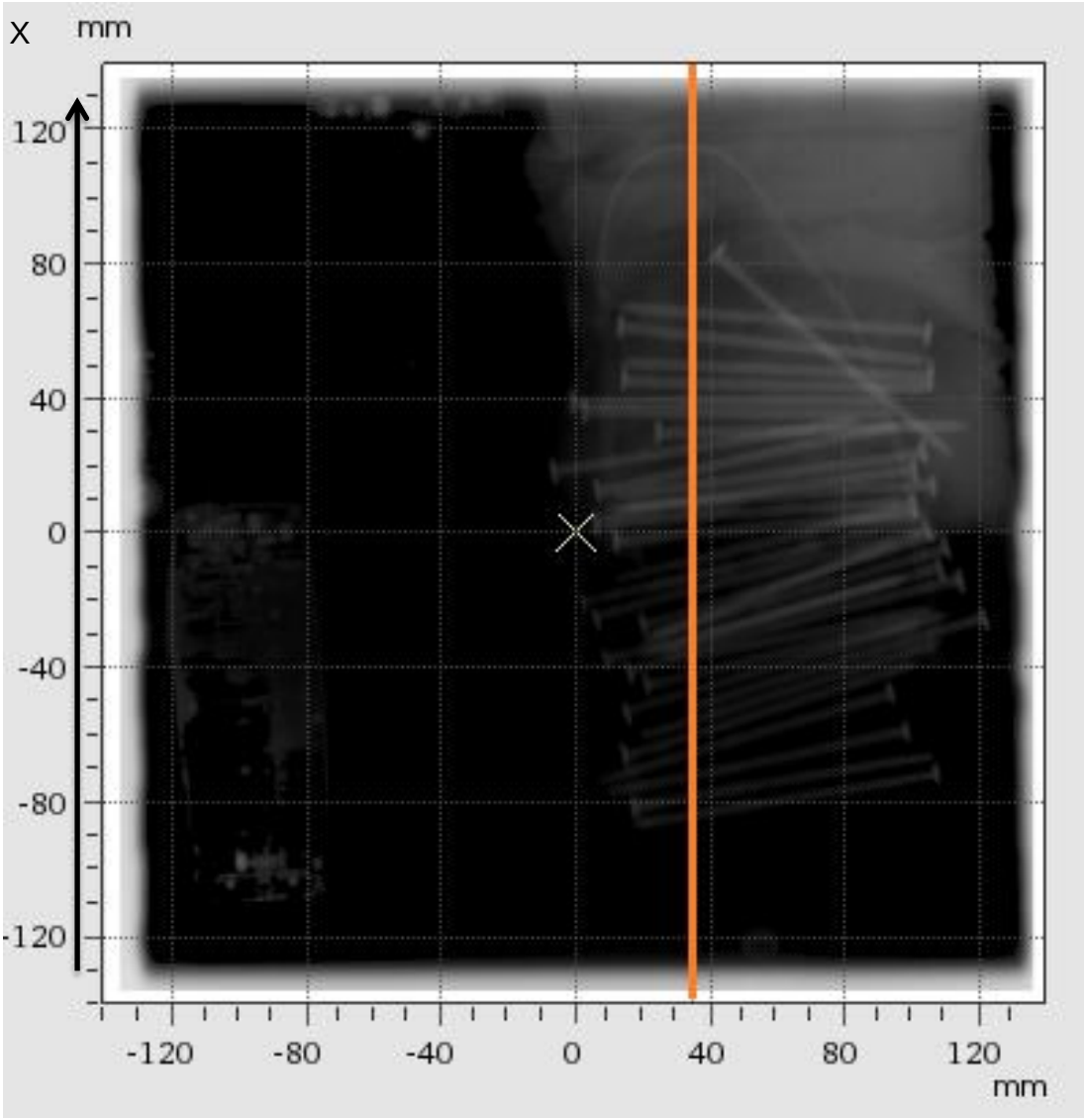



**Figure 21: An image of the briefcase using the Linac EPID**

**Table 5: Visible materials using the Linac.**

| Items | Visible | Comment |
|---|---|---|
| Putty | Yes | |
| Nails | Yes | All the nails were visible |
| Wires | No | Only the tripwire under putty the was visible |
| Cell phone | Yes | Some components of the phone were slightly visible |

| | | |
|---|---|---|
| Circuit board | Yes | The elements on the board were not visible |
| Battery | Yes | The cylindrical cells in the battery were all visible |
| Underlying/overlying material | Yes | Most underlying materials were visible |
| Switches | No | Only switch 1 was slightly visible |
| Detonator | No | |

Figure 22 displays a graph showing the data collected from the image taken using the EPID. The x-axis coordinates in Figure 22 correspond to the coordinates of the vertical line in Figure 21. The fall out in intensity levels at the ends of the graph is the edge of the briefcase. The nails underneath the putty are shown on the graph (from around 0 mm to about ± 70 mm), a reflection of what was seen in Figure 21. This modality would be most suitable in a situation where there are high Z materials concealed or obstructing other contents in the object being imaged.

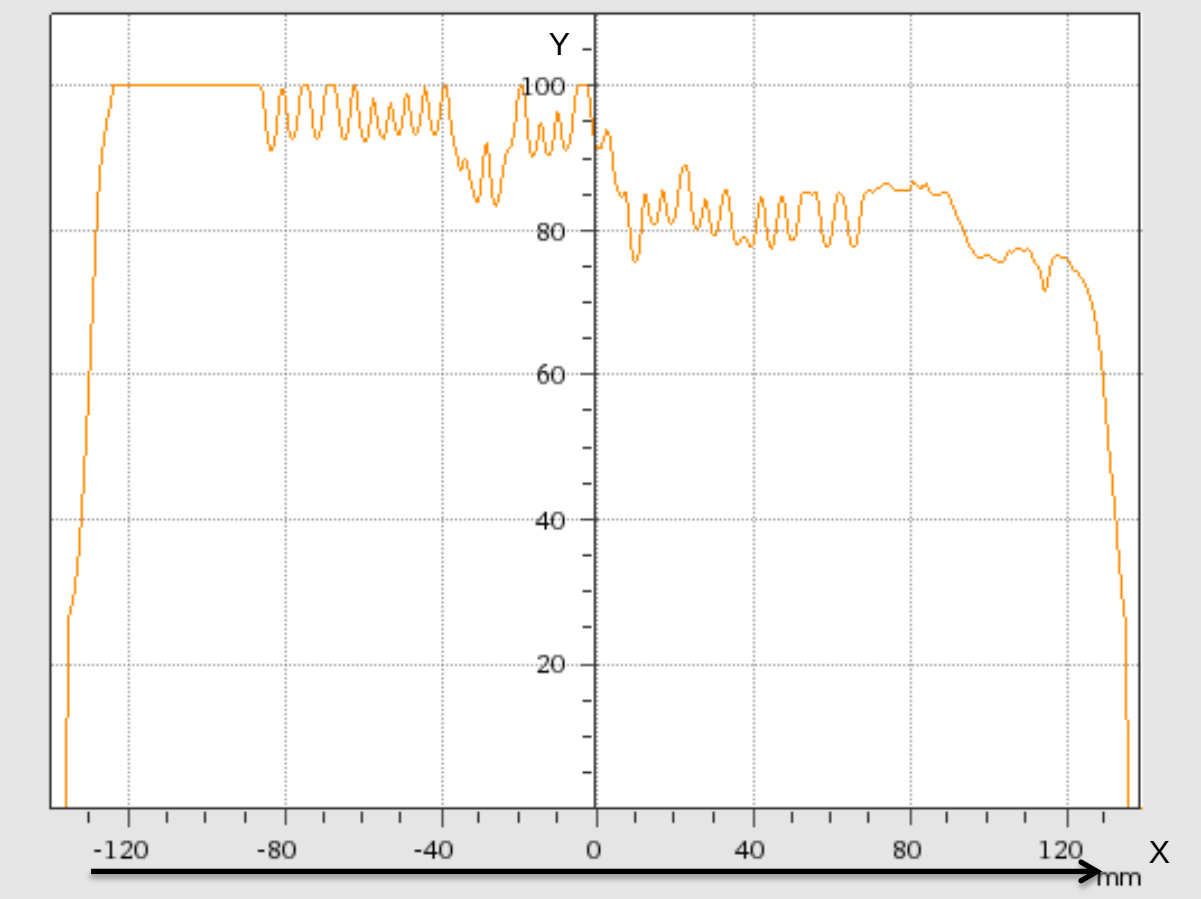



**Figure 22: A graph showing optical transmission from the EPID imager.**

### 4.2.3 Cobalt-60

The Gafchromic film used at the $^{60}$Co teletherapy machine was exposed for 24 minutes. Some materials were clearly seen on the Gafchromic film (putty, nails including those hidden under the putty, cell phone, and battery) however the wires and low density materials were not visible. Kodak ready pack film produced low contrast and poor resolution.

Figure 23 shows an image of the Fuji film used at the $^{60}$Co teletherapy machine. Observable on the Fuji film are the nails, putty, cell phone, batteries and the circuit board. Table 6 lists all the materials visible. Figure 24 displays a graph of the optical transmission of the film in Figure 23. The Fuji film had a uniform shade of grey giving low contrast and good spatial resolution. The fact that the source of radiation was not a point source and the Compton effect being independent of atomic number resulted

in the uniform shade of grey in the image and similar optical transmission on the graph. This modality would be ideal in circumstances where deep penetration and good spatial resolution are required, and where contrast is of little importance.

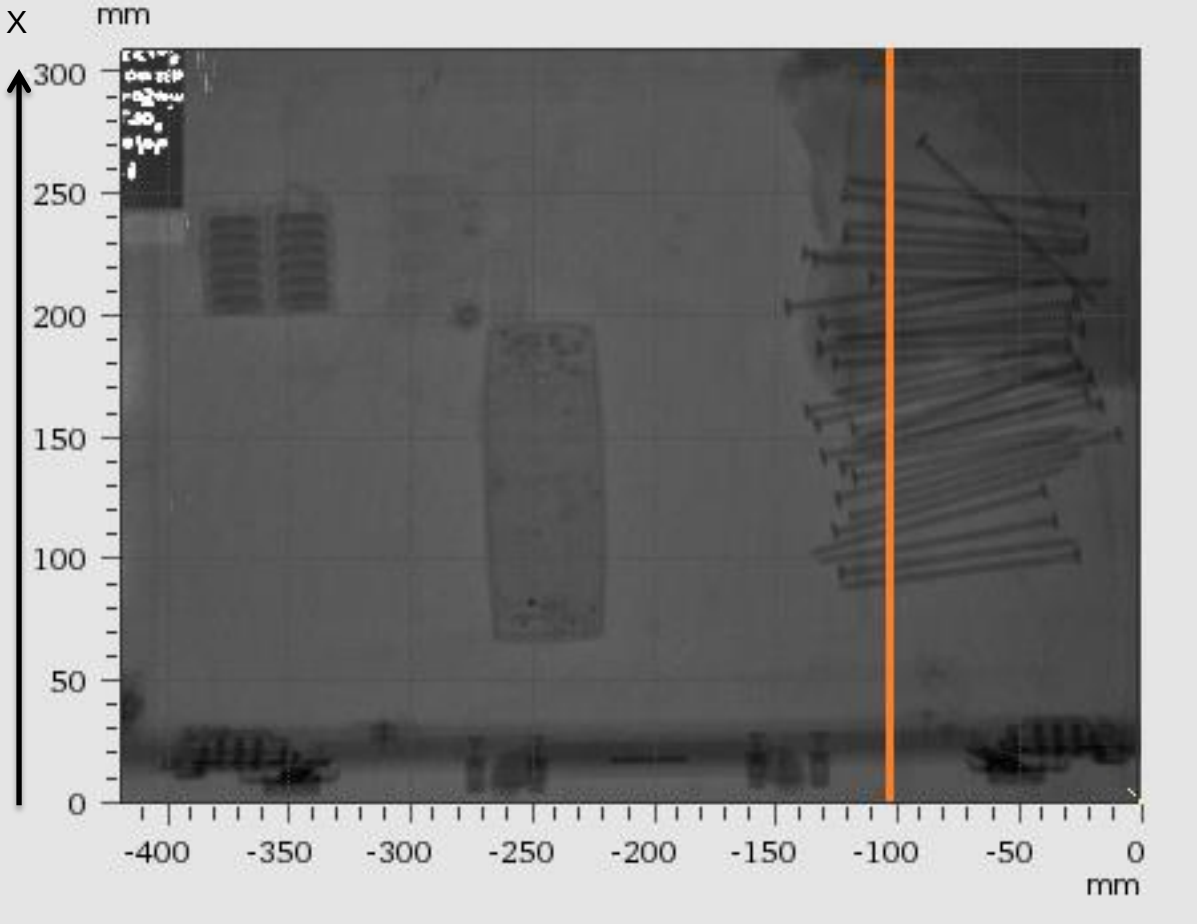



**Figure 23: An image of the briefcase using the $^{60}$Co teletherapy machine and Fuji film.**

**Table 6: Materials visible using the $^{60}$Co teletherapy machine**

| Items | Visible | Comment |
|---|---|---|
| Putty | Yes | |
| Nails | Yes | All the nails were visible |
| Wires | No | |
| Cell phone | Yes | Components of the phone were visible |
| Circuit board | Yes | The elements on the board were visible |
| Battery | Yes | The cylindrical cells in the battery were all visible |
| Underlying/overlying material | Yes | |
| Switches | No | Only switch 1 was slightly visible |
| Detonator | No | |

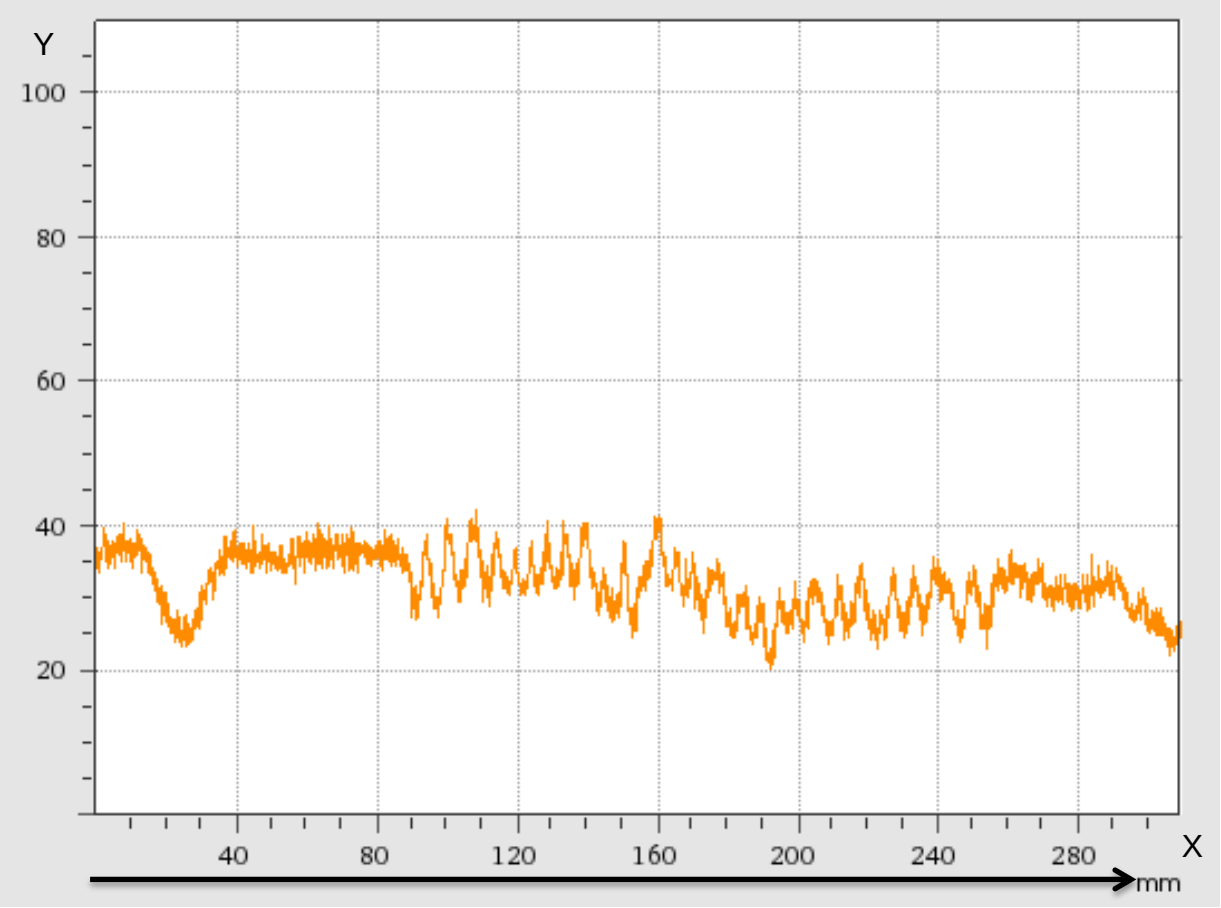



**Figure 24: A graph showing optical transmission from Fuji film using the $^{60}$Co teletherapy.**

### 4.2.4 Orthovoltage

Figure 25 is a combined image using 4 Kodak films obtained while imaging the briefcase. The energy used for the films was 300 $kV_p$ generated with a tube current of 8 mA for 300 MU. All the materials were visible, easily distinguished and are listed in Table 7. The difference in signal intensity was evident demonstrating good contrast on the film, a quality which lacked with the other modalities used in this study. High spatial resolution was attained with tiny materials visible on the film. The effects of photoelectric effect and Compton effect were present unlike at the other modalities where one process was dominant.

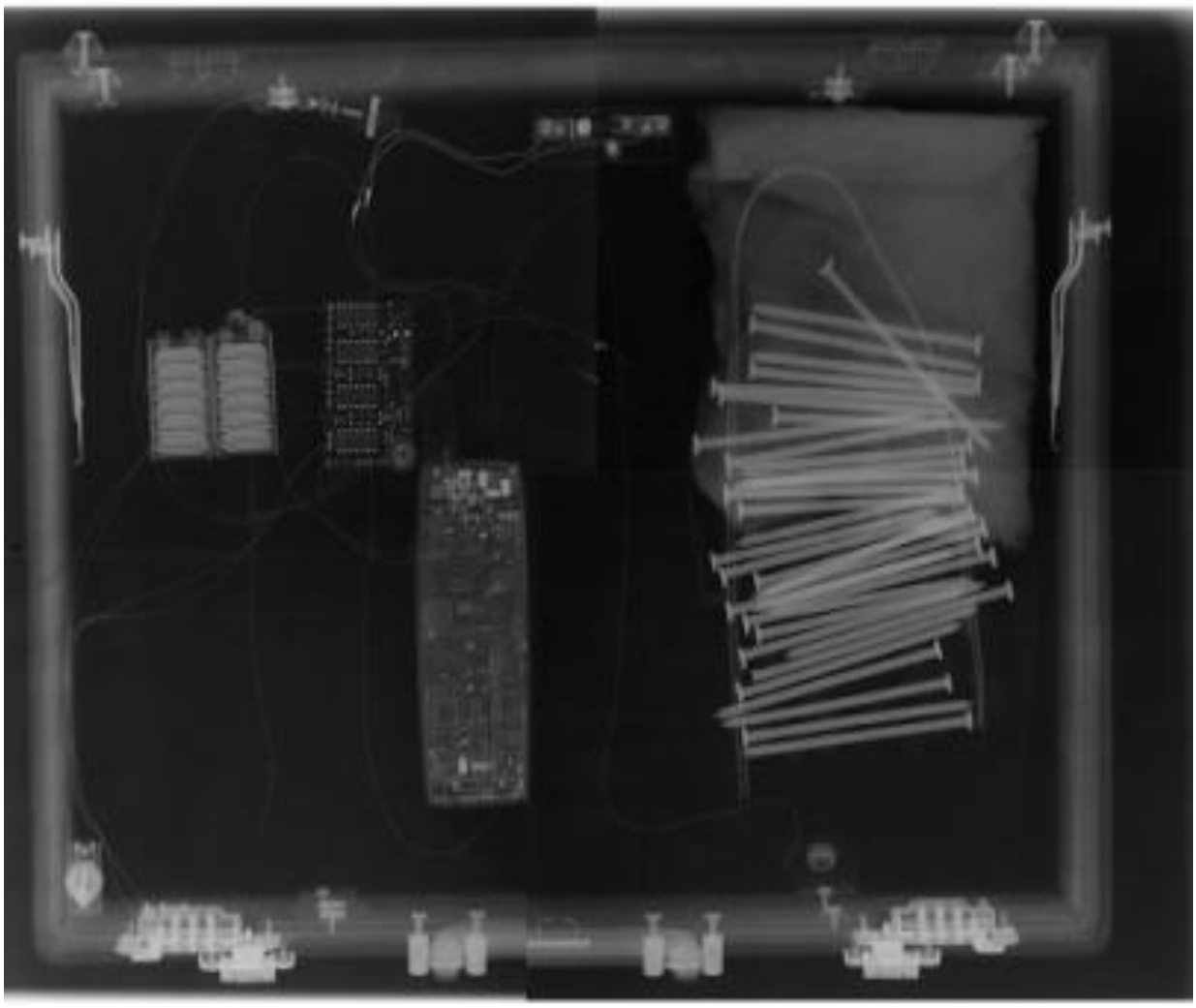


**Figure 25: An image showing combined Kodak film images from the orthovoltage teletherapy machine at 300 $kV_p$.**

**Table 7: Materials observed using the orthovoltage teletherapy machine.**

| Items | Visible | Comment |
|---|---|---|
| Putty | Yes | The uneven shape of the putty was visible |
| Nails | Yes | |
| Wires | Yes | |
| Cell phone | Yes | Components inside the mobile phone were visible |
| Circuit board | Yes | The elements on the board were visible |

| | | |
|---|---|---|
| Battery | Yes | The cylindrical cells in the battery were all visible |
| Underlying/overlying material | Yes | Overlying wires and hidden nails were visible |
| Switches | Yes | |
| Detonator | Yes | The materials in the detonator could be seen |

The detonator is one of the most crucial elements in an IED, it is used to initiate the main charge, hence detecting and identifying the detonator was important. Once it is identified the IED may be safely disarmed. The detonator was not visible using the Toshiba medical simulator, Linac or $^{60}$Co teletherapy machine and was slightly visible using the orthovoltage teletherapy machine.

In order to examine the small detail on the image in Figure 25, the image was magnified and focused on the detonator. Figure 26 is an image of the Kodak film displaying only the detonator (highlighted in red) and surrounding nails, cropping out the rest of the briefcase. The electric match inside the detonator could be seen from the connecting wires (traced in green and yellow) in Figure 26. The graph in Figure 27 shows the optical transmission on the film. The intensity levels correspond to the magnified image only, the data is collected from the orange horizontal line (from point 195 mm to 240 mm). There was variation in the height and width of the peaks. On the graph, the square box represents the region where the electric match in the detonator was located, the electric match lies in the range from 220 mm to 223 mm.

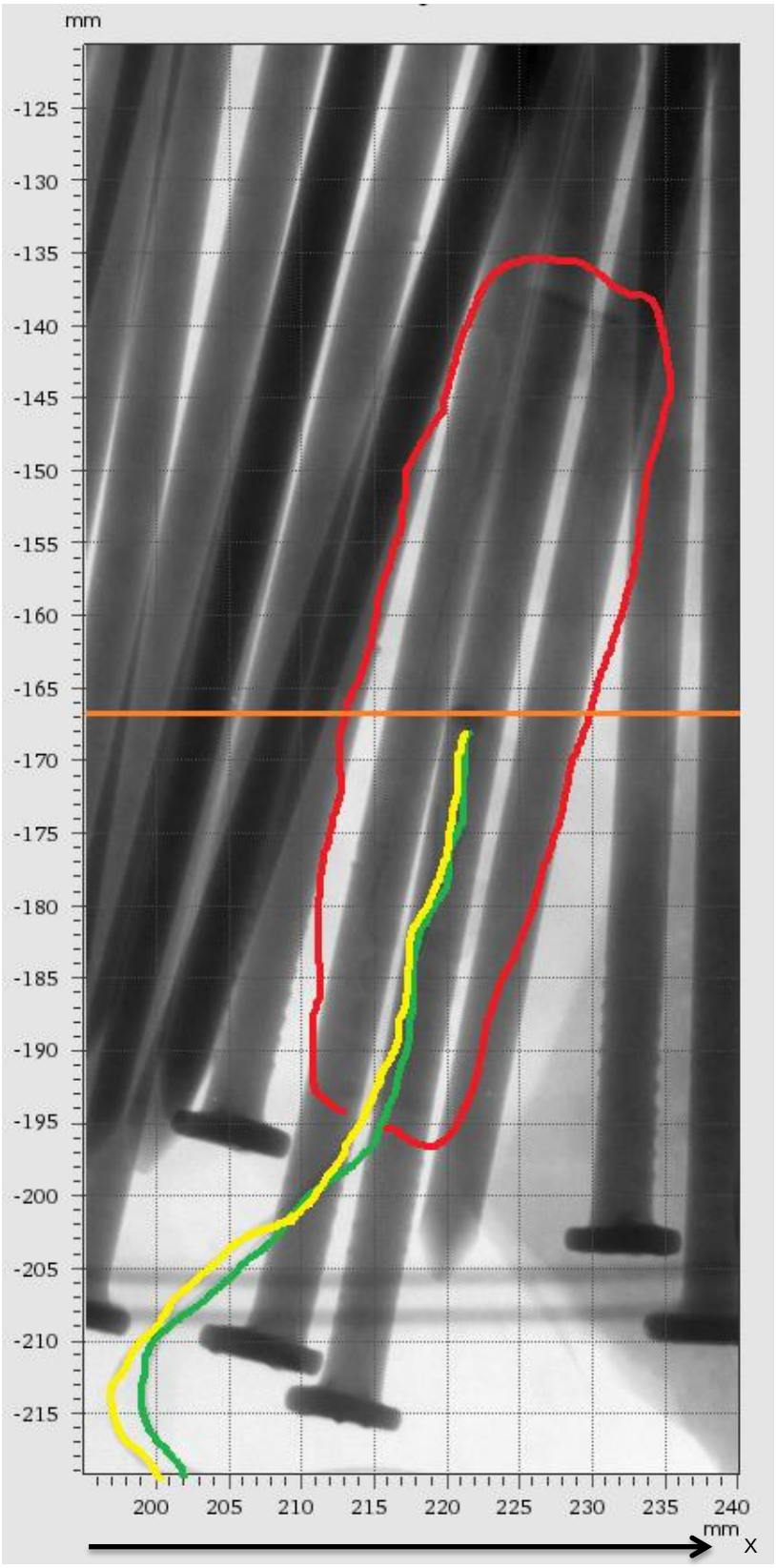



**Figure 26: An image of the Kodak film displaying the detonator, highlighted in red is the region where the detonator is positioned, traced in green and yellow are the wires connected to the electric match inside the detonator.**

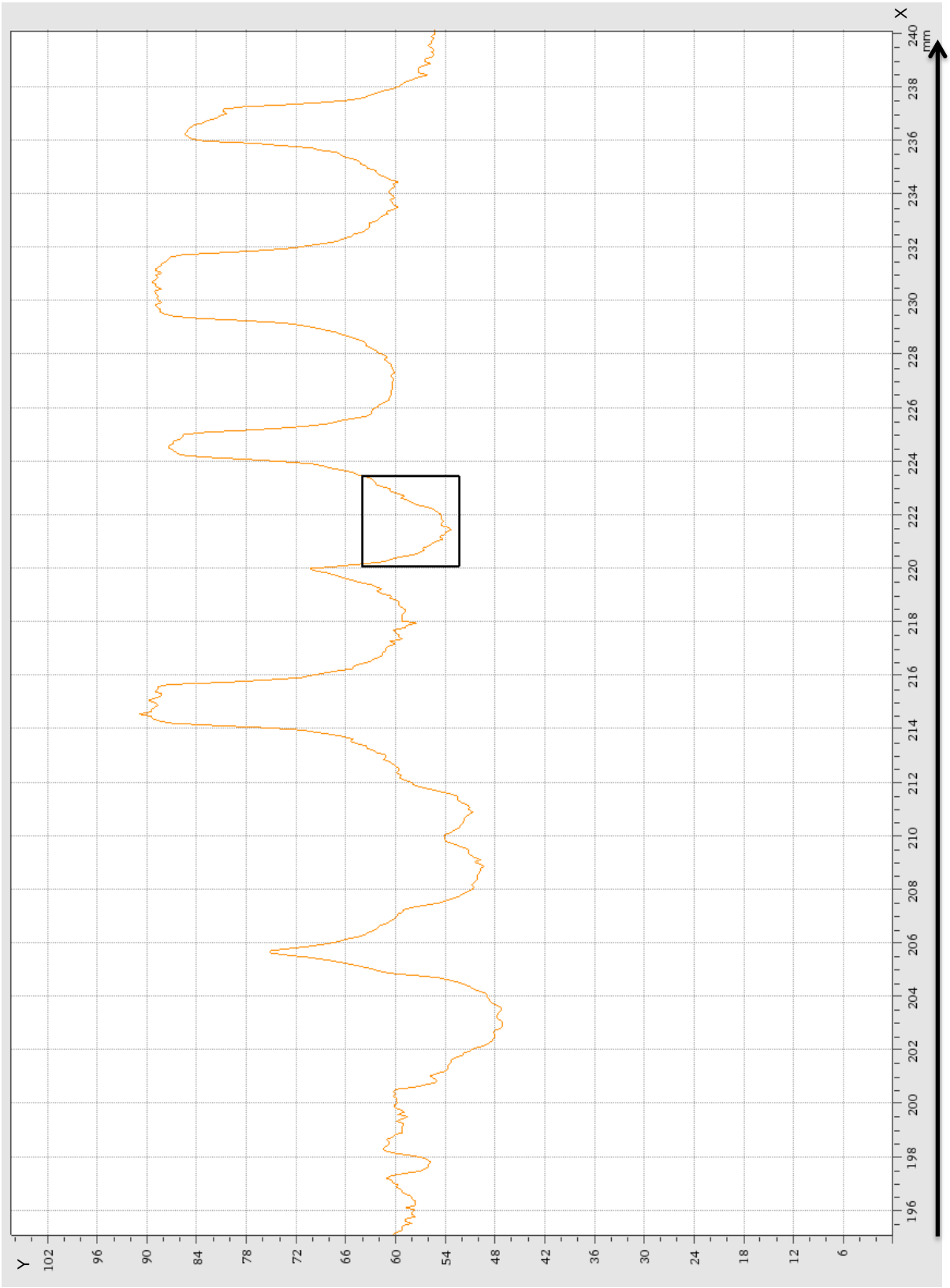



**Figure 27: A graph showing optical transmission on Kodak film using 300 $kV_p$ and 8 mAs, the square box on the graph represents the region where the electric match inside the detonator was located.**

### 4.2.5 CT

Figure 28 is a cross section of the IED from the CT scanner; circled in red is a cross section of the detonator. The CT machine produced poor images of the briefcase. 3D reconstruction and good quality digital images were expected at this modality. The materials in the briefcase were not clearly reproduced in 3D. There are a variety of reasons which could have caused the poor image quality from the CT. The machine defaults to a clinical protocol for any scanned object, which was probably not appropriate to the briefcase. The high attenuation of the foreign (non-medical) materials in the briefcase led to streak artefacts on the image.

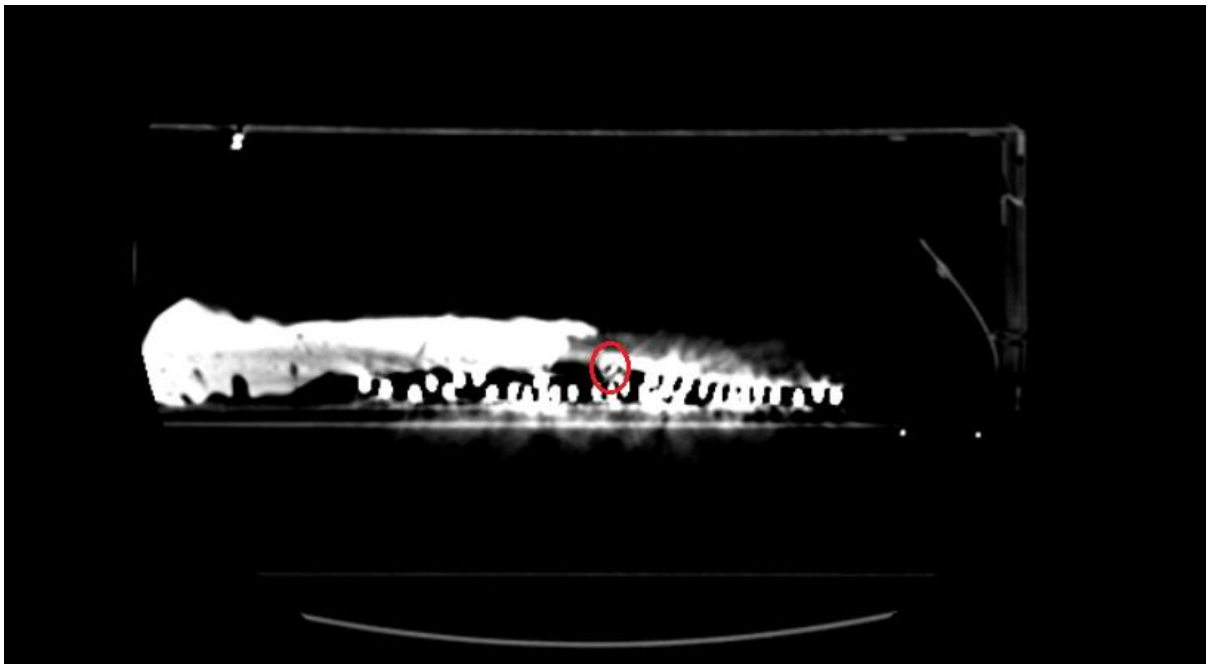


**Figure 28: A cross section of the briefcase using the CT scanner, circled in red is a cross section of the detonator.**

## 4.3 Summary table of results

An overview of the results obtained from the study is presented in Table 8.

**Table 8: A summary table of the visibility of each of the components in the briefcase at each modality.**

| | Visible | | | |
|---|---|---|---|---|
| **Items** | **Toshiba medical simulator** | **Linac** | **$^{60}$Co teletherapy machine** | **Orthovoltage teletherapy machine** |
| Putty | Yes | Yes | Yes | Yes |
| Nails | Not all | Yes | Yes | Yes |
| Wires | Yes | No | No | Yes |
| Cell phone | Yes | Yes | Yes | Yes |
| Circuit board | Yes | Yes | Yes | Yes |
| Battery | Yes | Yes | Yes | Yes |
| Underlying material | No | Yes | Yes | Yes |
| Switches | Yes | No | No | Yes |
| Detonator | No | No | No | Yes |

# 5. CONCLUSION

All the imaging modalities used in this study provided an image of the concealed IED, and each modality had a unique image quality. The Simulator provided high contrast and low spatial resolution however not all materials were visible. The Linac and $^{60}$Co teletherapy machine penetrated deeply into the materials showing underlying and overlying materials, with the $^{60}$Co teletherapy machine displaying good spatial resolution and low contrast.

The medical imaging technology at the Charlotte Maxeke Johannesburg Academic Hospital with the best potential for identifying the concealed energetic materials in the device studied in this work, was the orthovoltage teletherapy machine using the Kodak X-Omat V ready pack film as a detector. This system's detection ability was evaluated experimentally using an inert dummy IED and investigating an energy range from 95 $kV_p$ to 300 $kV_p$. 300 $kV_p$ produced an excellent image quality (good contrast and high spatial resolution). The variation in contrast on the film could easily be seen on the graph in Figure 27. This modality produced a detailed image of the briefcase, showing all the materials including overlying and underlying materials. The detonator was identified using this modality.

Imaging explosive materials may be very hazardous. However, with the variety of imaging technologies available in hospitals, inert dummy experiments can be evaluated. A prototype similar to the most promising technology can be developed for further studies using explosive materials. Technology can never be a solution to all the difficulties arising from terrorist attacks, but it provides useful tools which help minimise the threat in order to save civilian lives [28].

# 6. RECOMMENDATIONS

The orthovoltage teletherapy machine showed potential for identifying concealed objects. Further investigations should be done using an X-ray source similar to the orthovoltage teletherapy machine where other configurations of explosives should be tested. Blind detection of an IED would show the true potential of the orthovoltage modality.

Further research should be performed using non-clinical CT machines that do not use pre-set clinical scanning protocols. Such systems could help in locating and identifying concealed IED materials by providing the electron density of each material in the scanned object. In addition, CT imaging could provide multiplanar- and 3D-reconstruction of an IED threat.

# 7. REFERENCES


1. The Evolution of Improvised Explosive Devices (IEDs) | Brookings Institution [Internet]. Brookings. 2001 [cited 2016 Sep 23]. Available from: https://www.brookings.edu/articles/the-evolution-of-improvised-explosive-devices-ieds/

2. English R, Oppenheimer A. the Bombs and the Bullets: a History of Deadly Ingenuity''. 2009;

3. Gill P, Horgan J, Lovelace J. Improvised explosive device: The problem of definition. Stud Confl Terror. 2011;34(9):732–48.

4. Buffler A. Contraband detection with fast neutrons. Radiat Phys Chem. 2004;71(3):853–61.

5. Gottfried JL, Harmon RS, Munson CA, Winkel Jr RJ, Miziolek AW. Detection of Energetic Materials and Explosive Residues With Laser-Induced Breakdown Spectroscopy: 1. Laboratory Measurements. DTIC Document; 2007.

6. IED Components Analysis [Internet]. Assess Africa. 2016 [cited 2016 Nov 14]. Available from: http://www.assessafrica.com/analytics/

7. IED Attack Fact Sheet | Homeland Security [Internet]. [cited 2016 Jul 2]. Available from: https://www.dhs.gov/publication/ied-attack-fact-sheet

8. Halder R. BRUSSELS BOMBINGS: IDENTIFYING POTENTIAL CAUSES. Cent Air Power Stud. 2016 Apr 1;4.

9. Revill J. Improvised Explosive Devices: The Paradigmatic Weapon of New Wars. Springer; 2016. 149 p.

10. Overton I. Material Harm: A review of IED components and measures to prevent their spread. Action Armed Violence. 2014;

11. Explosive Violence Monitor 2015 [Internet]. AOAV. [cited 2016 Dec 2]. Available from: https://aoav.org.uk/explosiveviolence/explosive-weapons-monitor-2015/

12. Hutchinson JP, Evenhuis CJ, Johns C, Kazarian AA, Breadmore MC, Macka M, et al. Identification of inorganic improvised explosive devices by analysis of postblast residues using portable capillary electrophoresis instrumentation and indirect photometric detection with a light-emitting diode. Anal Chem. 2007;79(18):7005–13.

13. Parmeter JE. The challenge of standoff explosives detection. In IEEE; 2004. p. 355–8.

14. Singh S, Singh M. Explosives detection systems (EDS) for aviation security. Signal Process. 2003 Jan;83(1):31–55.

15. Bushberg JT, Boone JM. The essential physics of medical imaging. 3rd ed. Philadelphia: Lippincott Williams & Wilkins; 2011.

16. Dance D, Christofides S, Maidment A, McLean I, Ng K. Diagnostic radiology physics: A handbook for teachers and students. Vienna: International Atomic Energy Agency; 2014.

17. UNIDIR. Addressing Improvised Explosive Devices Options and Opportunities to Better Utilize UN Processes and Actors. In 2015.

18. Zentai G. X-ray imaging for homeland security. Int J Signal Imaging Syst Eng. 2010;3(1):13–20.

19. Zukas JA, Walters W, Walters WP. Explosive Effects and Applications. Springer Science & Business Media; 2002. 1458 p.

20. Hill J. Evolution of Bombings against Transportation Infrastructure. J Forensic Sci Criminol. 2016 Sep 31;4(4):404.

21. Zhou M, Li Z, Zhou Z, Zhang T, Wu B, Yang L, et al. Antistatic Modification of Lead Styphnate and Lead Azide for Surfactant Applications. Propellants Explos Pyrotech. 2013 Aug 1;38(4):569–76.

22. Initiation Systems [Internet]. Trace fire and safety. [cited 2017 Oct 18]. Available from: http://www.tracefireandsafety.com/VFRE-99/Recognition/Initiation/initiation.htm

23. Buffler A, Tickner J. Detecting contraband using neutrons: challenges and future directions. Radiat Meas. 2010;45(10):1186–92.

24. Bushberg JT. The AAPM/RSNA physics tutorial for residents. X-ray interactions. RadioGraphics. 1998 Mar 1;18(2):457–68.

25. Hendee WR, Ritenour E. Medical Imaging Physics. Wiley-Liss. Inc N Y. 2002;

26. Thayalan K. The Physics of Radiology and Imaging. JP Medical Ltd; 2014. 428 p.

27. Khan FM, Gibbons JP. Khan's the physics of radiation therapy. Lippincott Williams & Wilkins; 2014.

28. Fainberg A. Explosives Detection for Aviation Security. Sci Wash. 1992 Mar 20;255(5051):1531.

29. Hussein EM, Waller EJ. Review of one-side approaches to radiographic imaging for detection of explosives and narcotics. Radiat Meas. 1998;29(6):581–91.

30. Kolkoori S, Wrobel N, Osterloh K, Zscherpel U, Ewert U. Novel X-ray backscatter technique for detection of dangerous materials: application to aviation and port security. J Instrum. 2013;8(09):P09017.

31. Callerame J. X-ray backscatter imaging: Photography through barriers. Powder Diffr. 2006 Jun;21(2):132–5.

32. Lalleman AS, Ferrand G, Rossé B, Thfoin I, Wrobel R, Tabary J, et al. A dual X-ray backscatter system for detecting explosives: Image and discrimination of a suspicious content. In: 2011 IEEE Nuclear Science Symposium Conference Record. 2011. p. 299–304.

33. Speller R. Radiation-based security. Radiat Phys Chem. 2001;61(3):293–300.

34. IAEA. Quality Assurance Programme for Computed Tomography: Diagnostic and Therapy Applications. 2012 [cited 2017 Jun 11]; Available from: http://www-pub.iaea.org/books/IAEABooks/8751/Quality-Assurance-Programme-for-Computed-Tomography-Diagnostic-and-Therapy-Applications

35. Whetstone ZD, Kearfott KJ. A review of conventional explosives detection using active neutron interrogation. J Radioanal Nucl Chem. 2014 Sep;301(3):629–39.

36. Gozani T. Novel Applications of Fast-Neutron Interrogation Methods. Nucl Instrum Methods Phys Res Sect -Accel Spectrometers Detect Assoc Equip. 1994 Dec 30;353(1–3):635–40.

37. Gozani T. A review of neutron based non-intrusive inspection techniques. Ancore Corp St Clara CA USA. 2002;

38. Haley LV, Hallowell SF. Laser based explosives detection. In: Proceedings IEEE 34th Annual 2000 International Carnahan Conference on Security Technology (Cat No00CH37083). 2000. p. 207–17.

39. Mayles P, Nahum A, Rosenwald J-C. Handbook of radiotherapy physics: theory and practice. CRC Press; 2007.

40. Das IJ. Radiographic Film. Clin Dosim Radiother AAPM Summer Sch. 2009;865–89.

41. Soares C, Trichter S, Devic S. Radiochromic film. Clin Dosim Radiother AAPM Summer Sch. 2009;759–813.

42. Seco J, Clasie B, Partridge M. Review on the characteristics of radiation detectors for dosimetry and imaging. Phys Med Biol. 2014;59(20):R303.

43. Njeh CF, Caroprese B, Desai P. A simple quality assurance test tool for the visual verification of light and radiation field congruent using electronic portal images device and computed radiography. Radiat Oncol Lond Engl. 2012 Mar 27;7:49.

44. Rowshanfarzad P, McGarry CK, Barnes MP, Sabet M, Ebert MA. An EPID-based method for comprehensive verification of gantry, EPID and the MLC carriage positional accuracy in Varian linacs during arc treatments. Radiat Oncol Lond Engl [Internet]. 2014 Nov 26;9. Available from: https://www.ncbi.nlm.nih.gov/pmc/articles/PMC4252011/

45. PTW: Overview [Internet]. PTW. [cited 2017 Nov 22]. Available from: http://www.ptw.de/2320.html

46. Nyathi T. Dose optimization in diagnostic radiology. 2012;

47. Das IJ, Cao M, Cheng C-W, Misic V, Scheuring K, Schule E, et al. A quality assurance phantom for electronic portal imaging devices. J Appl Clin Med Phys. 2011;12(2).

48. EPID QA [Internet]. wienkav. [cited 2017 Nov 22]. Available from: http://www.wienkav.at/kav/kfj/91033454/physik/html/epidQA_image_registration.htm

49. Chetty IJ, Charland PM. Investigation of Kodak extended dose range (EDR) film for megavoltage photon beam dosimetry. Phys Med Biol. 2002;47(20):3629.

50. GafchromicVR E. Self-developing film for radiotherapy dosimetry. ISP White Pap. 2010;